

University of Windsor  
**Scholarship at UWindsor**

---

[Electronic Theses and Dissertations](#)

[Theses, Dissertations, and Major Papers](#)

---

1982

## A study of the E.P.R. spectrum of potassium sulfate : copper(2+).

David John. Unwin  
*University of Windsor*

Follow this and additional works at: <https://scholar.uwindsor.ca/etd>

---

### Recommended Citation

Unwin, David John., "A study of the E.P.R. spectrum of potassium sulfate : copper(2+)." (1982). *Electronic Theses and Dissertations*. 792.  
<https://scholar.uwindsor.ca/etd/792>

This online database contains the full-text of PhD dissertations and Masters' theses of University of Windsor students from 1954 forward. These documents are made available for personal study and research purposes only, in accordance with the Canadian Copyright Act and the Creative Commons license—CC BY-NC-ND (Attribution, Non-Commercial, No Derivative Works). Under this license, works must always be attributed to the copyright holder (original author), cannot be used for any commercial purposes, and may not be altered. Any other use would require the permission of the copyright holder. Students may inquire about withdrawing their dissertation and/or thesis from this database. For additional inquiries, please contact the repository administrator via email ([scholarship@uwindsor.ca](mailto:scholarship@uwindsor.ca)) or by telephone at 519-253-3000 ext. 3208.

## CANADIAN THESES ON MICROFICHE

I.S.B.N.

## THESES CANADIENNES SUR MICROFICHE



National Library of Canada  
Collections Development Branch

Canadian Theses on  
Microfiche Service

Ottawa, Canada  
K1A 0N4

Bibliothèque nationale du Canada  
Direction du développement des collections

Service des thèses canadiennes  
sur microfiche

### NOTICE

The quality of this microfiche is heavily dependent upon the quality of the original thesis submitted for microfilming. Every effort has been made to ensure the highest quality of reproduction possible.

If pages are missing, contact the university which granted the degree.

Some pages may have indistinct print especially if the original pages were typed with a poor typewriter ribbon or if the university sent us a poor photocopy.

Previously copyrighted materials (journal articles, published tests, etc.) are not filmed.

Reproduction in full or in part of this film is governed by the Canadian Copyright Act, R.S.C. 1970, c. C-30. Please read the authorization forms which accompany this thesis.

THIS DISSERTATION  
HAS BEEN MICROFILMED  
EXACTLY AS RECEIVED

### AVIS

La qualité de cette microfiche dépend grandement de la qualité de la thèse soumise au microfilmage. Nous avons tout fait pour assurer une qualité supérieure de reproduction.

S'il manque des pages, veuillez communiquer avec l'université qui a conféré le grade.

La qualité d'impression de certaines pages peut laisser à désirer, surtout si les pages originales ont été dactylographiées à l'aide d'un ruban usé ou si l'université nous a fait parvenir une photocopie de mauvaise qualité.

Les documents qui font déjà l'objet d'un droit d'auteur (articles de revue, examens publiés, etc.) ne sont pas microfilmés.

La reproduction, même partielle, de ce microfilm est soumise à la Loi canadienne sur le droit d'auteur, SRC 1970, c. C-30. Veuillez prendre connaissance des formules d'autorisation qui accompagnent cette thèse.

LA THÈSE A ÉTÉ  
MICROFILMÉE TELLE QUE  
NOUS L'AVONS RECUE

A STUDY OF THE E.P.R. SPECTRUM  
OF  $K_2SO_4$  :  $Cu^{2+}$

by



David John Unwin

A Thesis  
Submitted to the Faculty of Graduate Studies  
through the Department of Physics in  
Partial Fulfillment of the Requirements  
for the Degree of Master of Science  
at the University of Windsor

Windsor, Ontario

1982

## ABSTRACT

The system  $K_2SO_4:Cu^{2+}$  produces four sets of spectra and the previously uninvestigated weak set was studied by electron paramagnetic resonance methods.

The data were fitted to the spin Hamiltonian

$$H = S.g.H + S.A.I. + I.Q.I$$

using an exact diagonalization process and a multi-dimensional least squares method. The parameters were found to be (in crystallographic co-ordinates)

g <sub>xx</sub>	g <sub>yy</sub>	g <sub>zz</sub>
2.5396±.0001	2.1296± .0001	2.0920±.0001
g <sub>xy</sub>	g <sub>zx</sub>	g <sub>zy</sub>
0.1023±.0001	0.0347±.0001	0.0516±.0002
A <sub>xx</sub> . $10^{-4} \text{ cm}^{-1}$	A <sub>yy</sub>	A <sub>zz</sub>
205.3±0.9	19.9± 5.6	38.5±4.0
A <sub>xy</sub>	A <sub>zx</sub>	A <sub>zy</sub>
88.3±2.0	2.3±1.6	-36.9±4.5
Q <sub>x</sub> . $10^{-4} \text{ cm}^{-1}$	Q <sub>y</sub>	
20.6±2	3.8±0.6	

Diagonalization of g and A tensors show that they are highly non-coincident. This is due to a very low symmetry environment of the paramagnetic impurity. Reasonable agreement with a previously suggested charge compensation mode was also found.

 ACKNOWLEDGEMENTS

The author wishes to thank Dr. F. Holuj for his guidance during the work and Dr. M. Khan for x-ray crystallography enabling identification of axes.

## TABLE OF CONTENTS

	Page
<b>ABSTRACT</b>	iii
<b>ACKNOWLEDGEMENTS</b>	v
<b>LIST OF TABLES</b>	viii
<b>LIST OF FIGURES</b>	ix
<b>CHAPTER</b>	
I. INTRODUCTION AND PURPOSE OF EXPERIMENT	1
II. THE CRYSTAL STRUCTURE OF $K_2SO_4$	2
III. THEORY	4
A. Electron Paramagnetic Resonance	4
B. The Divalent Copper Ion	6
C. The Complete Hamiltonian	7
D. The Spin Hamiltonian	9
IV. INSTRUMENTATION	12
A. K-Bond Spectrometer	12
(1) Klystron Stabilizer	12
(2) Microwave Circuit	14
(3) External Magnetic Field and Modulations	17
B. Proton Magnetometer	17
V. EXPERIMENTAL PROCEDURE	
(1) Crystal Orientation	18
(2) Measurement of Magnetic Field	26
(3) Measurement of Microwave Frequency	28
VI. DEVELOPMENT OF COMPUTER PROGRAM	29
A. The Method	29

B.	The Flow Chart	34
C.	Rate of Convergence	37
VII.	DISCUSSION AND CONCLUSION	39
BIBLIOGRAPHY		48
APPENDIX	1. DATA	49
	2. Identification of Crystallographic axes	51
	3. Program used for calculating P(I)	52
	4. STCM: Similarity Transform Converts Matrix Elements to New Basis	55
	5. RTN 1: Main Subroutine	56
	6. CEIGEN - Computes Eigenvalues and Eigenrectors of Hemitian Matrix (double precision complex)	63
	7. DGMPRO: Matrix Multiplication of two general double precision matrices	64
	8. Diagonalization of g and A tensor	65
VITA AUCTORIS		68

LIST OF TABLES

	Page
IV. 1 Rate of Convergence	37
VII. 1 Spectral Parameters	40

LIST OF FIGURES

	Page
II. 1 Crystal Structure of $K_2SO_4$	3
IV. 1 Block Diagram of Spectrometer	13
IV. 3 Diagram of Microwave Detector and Balanced transformer	15
V. 1-3 Spectra along crystallographic axes	19, 20, 21
V. 4-6 Angular variation	23, 24, 25
V. 7 P.M.R. Probe	27
V. 8 P.M.R. Signal	28
VI. 1 Block diagram of Computer Program	35
VII. 1 Crystal Structure of $K_2SO_4$	42
VII. 3 Sereogram of g and A tensors	43

## CHAPTER I

### INTRODUCTION AND PURPOSE OF EXPERIMENT

Although the initial objective had been to study  $\text{LiK}_2\text{So}_4:\text{Cu}^{2+}$ , obtaining samples proved to be difficult and  $\text{K}_2\text{SO}_4:\text{Cu}^{2+}$  was investigated instead.

The course of searching for a crystal of  $\text{LiK}_2\text{So}_4$  with sufficient copper doping to produce strong electron paramagnetic resonance signals yielded crystals of  $\text{K}_2\text{SO}_4$  with extremely strong signals.

Although the spectrum of  $\text{K}_2\text{SO}_4:\text{Cu}^{2+}$  had previously been investigated by Abdulsabirov<sup>1</sup> and Freeman<sup>2</sup>, these investigations left open the questions of non coincident g and A tensor and although Abdulsabirov<sup>1</sup> had evaluated three sets of spectra, the charge compensation mechanism they suggested left open the possibility of a fourth mechanism and a set of weak lines had not been investigated by 1 or 2.

The purpose of the investigation was to evaluate the spectrum of this weak set and to check agreement with both the charge compensation mechanism suggested by 1 and the non-coincidences reported by 2. For this purpose crystals containing a single isotope  $\text{Cu}^{63}$  were prepared thus yielding a greater resolution since the relaxation times (spin-lattice) at 77°K were such that the  $\text{Cu}^{63}$  and  $\text{Cu}^{65}$  lines overlapped.

## CHAPTER II

### THE CRYSTAL STRUCTURE OF $K_2SO_4$

X-ray studies<sup>3</sup> have shown that  $K_2SO_4$  is orthorhombic with  $a=7.456\text{\AA}$ ,  $b=10.08\text{\AA}$ ,  $c=5.776\text{\AA}$  and has space group Pnam, ( $D_{2n}^{16}$ ).

Each unit cell contains 4 formula units and the  $SO_4$  groups form groups of symmetry related tetrahedra.

A diagram of the crystal structure is shown in fig. II.1 with a box around the unit cell.

The crystals were grown from aqueous solution by slow evaporation at room temperature and doped with  $Cu^{63}$  during growth.

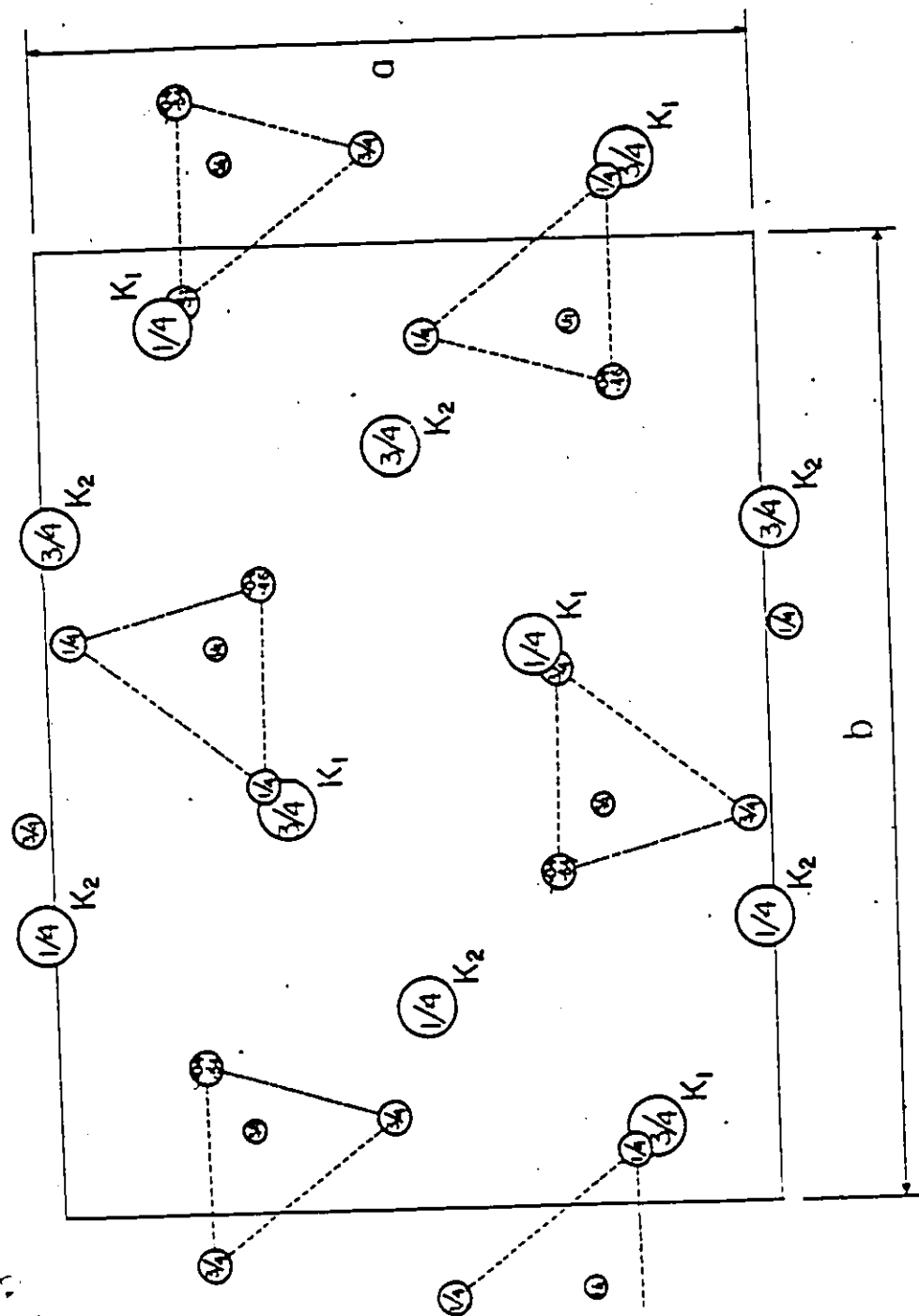


FIG II.1

## CHAPTER III

## THEORY

## A. Electron Paramagnetic Resonance

This phenomenon was first reported by Zavoyskiy<sup>4</sup> in 1945 and refers to the magnetic resonance of permanent magnetic dipole moments of electrons.

Paramagnetic centres may be produced in various ways, some of which are,

- 1.) Radicals in solids
- 2.) Radiation damage centres
- 3.) Molecule-like complexes in a solid matrix
- 4.) Paramagnetic impurities

In our case, 4), the paramagnetic impurity is a copper dopant  $\text{Cu}^{2+}$ .

If we consider the case of a single paramagnetic ion which is not interacting with other impurity ions via dipole-dipole interactions and has a single unpaired electron in an S state with a "spin-only" magnetic dipole moment of  $m_s g_s \beta$  ( $m_s = 1/2$ ,  $\beta$  is the Bohr magneton,  $g_s = g$  free electron), then in a magnetic field the spin degeneracy is resolved and the dipole may orient itself parallel or antiparallel to the external magnetic field with corresponding energies  $\pm \frac{1}{2} \beta g_s H$ , and this is the familiar Zeeman effect.

Considering an ensemble of such ions we may observe magnetic dipole transitions induced between these two levels by applying a high frequency magnetic field polarized perpendicularly to  $\mathbf{H}$  which satisfies the resonance condition.

$$\hbar\omega = g_S \mathbf{g}_H \cdot \mathbf{B}$$

Resonance absorption will then be observed corresponding to dipoles being shipped from parallel to antiparallel to  $\mathbf{H}$ .

Emission will also be induced although when the system remains in thermal equilibrium the population of  $\vec{\mu}$  dipole parallel to  $\mathbf{H}$  will exceed that of  $\vec{\mu}$  dipole antiparallel to  $\mathbf{H}$ , and a net absorption will occur.

Zeeman separations at 10KQ are typically  $0.01\text{cm}^{-1}$  and  $kT_{\text{room}} \sim 200\text{ cm}^{-1}$  and since it is the slight difference in populations which gives rise to observable transitions the absorption is enhanced at lower temperatures. Another advantage of lower temperatures is that a major source of E.P.R. line broadening is spin-lattice relaxation and since spin-lattice relaxation time generally increases at lower temperatures the line width is reduced.

Other effects which cause line broadening are spin-spin interactions and exchange effects, neither of which are important in our case.

The spectra discussed here were all recorded at liquid nitrogen temperature ( $77^\circ\text{ K}$ ).

Consider an ion having an orbitally non degenerate ground state with spin  $S$ . The "spin-only" interaction with an external magnetic field will be

$$= 2\beta \vec{H} \cdot \vec{S}$$

If  $\vec{H}$  is parallel to  $\vec{Z}$  then the term splits into  $(2S+1)$  equally spaced levels with energies  $2\beta HM_s$  and a separation  $2\beta H$  between adjacent levels.

Magnetic dipole transitions will have intensities proportional to

$$P_{\epsilon} = |\langle \psi_{\text{Final}} | (L_{\epsilon} + g_s S_{\epsilon}) | \psi_{\text{Initial}} \rangle|^2$$

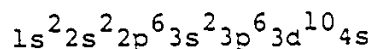
as a consequence of Fermi's Golden Rule. The subscript  $\epsilon$  denotes the component along the direction of the magnetic vector of the incident radiation. With  $P_{\epsilon}$  as above we have, ( $H=\text{Hz}$ )

$$P_x = P_y = S(S+1) - M_s(M_s+1)$$

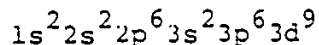
for the transition  $|SM_s\rangle \rightarrow |SM_{s+1}\rangle$  and  $P_x = P_y = P_z = 0$  for all other transitions. So we have the selection rule  $\Delta M_s = \pm 1$ . In practice this simple scheme is complicated by crystal field effects, spin-orbit coupling and hyperfine interactions. Hyperfine interaction between the electron and the magnetic moment of the nucleus results in a further splitting of each  $M_s$  level into  $(2I+1)$  levels.

#### B. The divalent Copper Ion

The ground state of the copper atom has the electronic configuration



Thus giving a  $^2S$  term, the divalent copper ion has a configuration



Resulting in a  $^2D$  term,  $L=2$ ,  $s=1/2$ . This can conveniently be treated as a hole in a closed 3d shell in the complementary scheme.

### C. The Complete Hamiltonian

The complete hamiltonian operator for a paramagnetic ion in a crystalline field and zero magnetic field is

$$= T + V_c + V_{so} + V_x + V_{ss} + V_{SI} + V_Q \quad (\text{III.1})$$

where;

$$T = \sum_k (p_k^2 / 2M)$$

is the total KE of the  $k^{\text{th}}$  electron with momentum  $p_k$  and mass  $M$  and the sum extends over all the electrons for the ion.

The Coulomb term  $V_c$  consists of

$$V_c = - \sum_k \frac{ze^2}{r_k} + \frac{1}{2} \sum_{i \neq j} \frac{e^2}{r_{ij}}$$

The first term is the Coulomb attraction between the  $k^{\text{th}}$  electron and the nucleus and the second term is the Coulomb interaction between electrons summed over all electrons in the ion. The factor of  $1/2$  eliminates double counting.

The  $V_{so}$  term is the contribution due to spin-orbit coupling and can be written as

$$V_{so} = \sum_{ij} \lambda_{ij} \vec{l}_i \cdot \vec{s}_j$$

Where  $i$  and  $j$  are summed over all electrons in the ion.

With Russell-Saunders coupling this becomes

$$\sum_i \vec{l}_i = \vec{L} \text{ and } \sum_i \vec{s}_i = \vec{s}$$

And so  $V_{SO}$  becomes

$$V_{SO} = \lambda \vec{L} \cdot \vec{s}$$

where  $\lambda$  is the spin-orbit coupling constant and depends on some radial integral.

$V_x$  represents the interaction between the paramagnetic ion and the crystal field potential

$$V_x = -\sum_k e \Phi(\vec{r}_k)$$

$V_{ss}$  represents the magnetic dipole-dipole interaction between electrons and in our case can be set equal to zero since we are dealing with a dilute impurity with a single hole.

$V_{SI}$  represents the magnetic interaction between unpaired electrons and the nuclear moments of both central ion and ligands. In our case no superhyperfine interaction was observed.

A full relativistic treatment of the interaction between an electron and the nuclear magnetic moment of the nucleus (see Griffith § 5.5.3) shows that the interaction adds a term

$$= 2\gamma \beta g_N \vec{l} \cdot \left\{ f(r^{-3} \vec{l} \cdot \vec{s} + 3r^{-5} (\vec{s} \cdot \vec{r}) \vec{r}) + r^{-2} \frac{df}{dr} (\vec{s} - r^{-2} (\vec{s} \cdot \vec{r}) \vec{r}) \right\} r$$

where  $f = 1 - \frac{E + eA_Q}{2mc^2}$  and is close to unity.

After a lot of heavy algebra and with the use of the replacement theorem of equivalent operators this can be written as (within a term):

$$H_m = \mu \left\{ \vec{L} \cdot \vec{I} - K(\vec{s} \cdot \vec{i}) + \xi [E(L+1)\vec{s} \cdot \vec{i} - \frac{3}{2}(\vec{L} \cdot \vec{s})(\vec{L} \cdot \vec{i})] \right\}$$

with,

$$P = 2\gamma \beta_N \langle r^{-3} \rangle$$

$\gamma$  depends on the nucleus in question and  $\beta_N$  is the nuclear magneton,

and,

$$\xi = \frac{2 + 1 - 4S}{S(2I-1) (2I+3) (2L-1)}$$

Within a  $d^n$  configuration there should not be a Fermi contribution of the form  $\vec{S} \cdot \vec{I}$  but configuration interaction means that there is always an unpaired spin density at the nucleus from s wave contributions which are mixed in by configuration interaction. This warrants the term  $K(\vec{S} \cdot \vec{I})$  but unfortunately there is no accurate way of calculating  $K$ .

$V_Q$  represents the quadrupole interaction between the nuclear and electronic quadrupole moments and can be written as the equivalent operator:

$$\vec{I} \cdot Q \cdot \vec{I}$$

Since in practice this is a small contribution, only diagonal elements are considered and application of  $\nabla \cdot \vec{E} = p$  gives the extra condition that  $\text{Tr}(Q) = 0$ . If only  $\Delta_{MI} = 0$  transitions are considered then  $\text{Tr}(Q)$  is in any case indeterminate since it only adds a constant  $\frac{1}{3}\text{Tr}(Q)I(I+1)$  to the Hamiltonian.

#### D. The spin Hamiltonian

The complete Hamiltonian as written in III.1 is too cumbersome to work with and in our case  $V_x$  is unknown.

For the fitting of the recorded spectra we make use of an equivalent Hamiltonian of the form:

$$H = \tilde{S} \cdot g \cdot \vec{H} + S \cdot A \cdot \vec{I} + \vec{I} \cdot Q \cdot \vec{I}$$

The first term is the electronic Zeeman term and the  $\tilde{S}$  "tensor" reflects anisotropy in the spectrum due to spin-orbit and crystal field effects. The  $\tilde{S}$  here is not the actual spin of the system but is an effective spin, often called "fictitious spin".  $(2S+1)$  is equal to the number of electronic levels in the ground state of the ion.

The second term describes the magnetic hyperfine interaction discussed earlier. The  $A$  "tensor" describes both the magnetic interaction and the Fermi contact interaction.

The third term is an equivalent operator form for the interaction between the electronic and nuclear quadrupole moments as discussed earlier. The restriction  $\text{Tr}(Q) = 0$  reduces the number of empirical factors needed to fit the spectrum since  $\text{Tr}(Q)$  only adds a constant  $\frac{1}{3}\text{Tr}(Q)I(I+1)$  to  $H$  if  $\Delta_{MI} = 0$  only transitions are considered. Its inclusion is warranted by the fact that at certain orientations  $\Delta_{MI} = \pm 1$  "forbidden" transitions are easily seen. This is because this non linear term in  $I$  means  $M_I$  is no longer a good quantum number.

If we choose a frame of reference which diagonalizes the  $g$  "tensor" then the Zeeman term can be written as

$$H = (S_x, S_y, S_z) \cdot \begin{pmatrix} g_x & 0 & 0 \\ 0 & g_y & 0 \\ 0 & 0 & g_z \end{pmatrix} \cdot \begin{pmatrix} H_x \\ H_y \\ H_z \end{pmatrix}$$

$$= (g_x S_x H_x + g_y S_y H_y + g_z S_z H_z)$$

Similarly for the  $A$  "tensor"

$$H = (A_x' S_x' I_x' + A_y' S_y' I_y' + A_z' S_z' I_z')$$

Although for low symmetries it may not be possible to diagonalize  $g$  and  $A$  simultaneously as we shall see.

## CHAPTER IV

### INSTRUMENTATION

#### A. K-Band Spectrometer

The K-band spectrometer used was of balanced bridge design, using a circulator, with the microwave frequency stabilized against the sample cavity. A block diagram is shown in fig. IV.1. The microwave power was supplied by a Varian model VA98E reflex klystron producing 30mW of power.

##### (1) Klystron Stabilizer

The klystron frequency was stabilized to the cavity resonant frequency using a Teltronic model KSLP Klystron Stabilizer. The stabilizer works on the principle of automatic frequency control (A.F.C.). A sine wave modulation of approximately 70 KHz was impressed on the reflector voltage thus causing a small amount of frequency modulation. If the Klystron frequency is tuned at or near the cavity resonant frequency, the output detected by the A.F.C. signal is amplified and then applied to the phase sensitive detector (P.S.D.) built into the stabilizer, which compares the signal with the original modulation signal. The result is a D.C. error voltage with a polarity and magnitude proportional to the difference between the klystron oscillator frequency and the resonant frequency of the cavity. The error voltage is applied to the reflector of klystron in such a manner that the klystron frequency is pulled back to the frequency

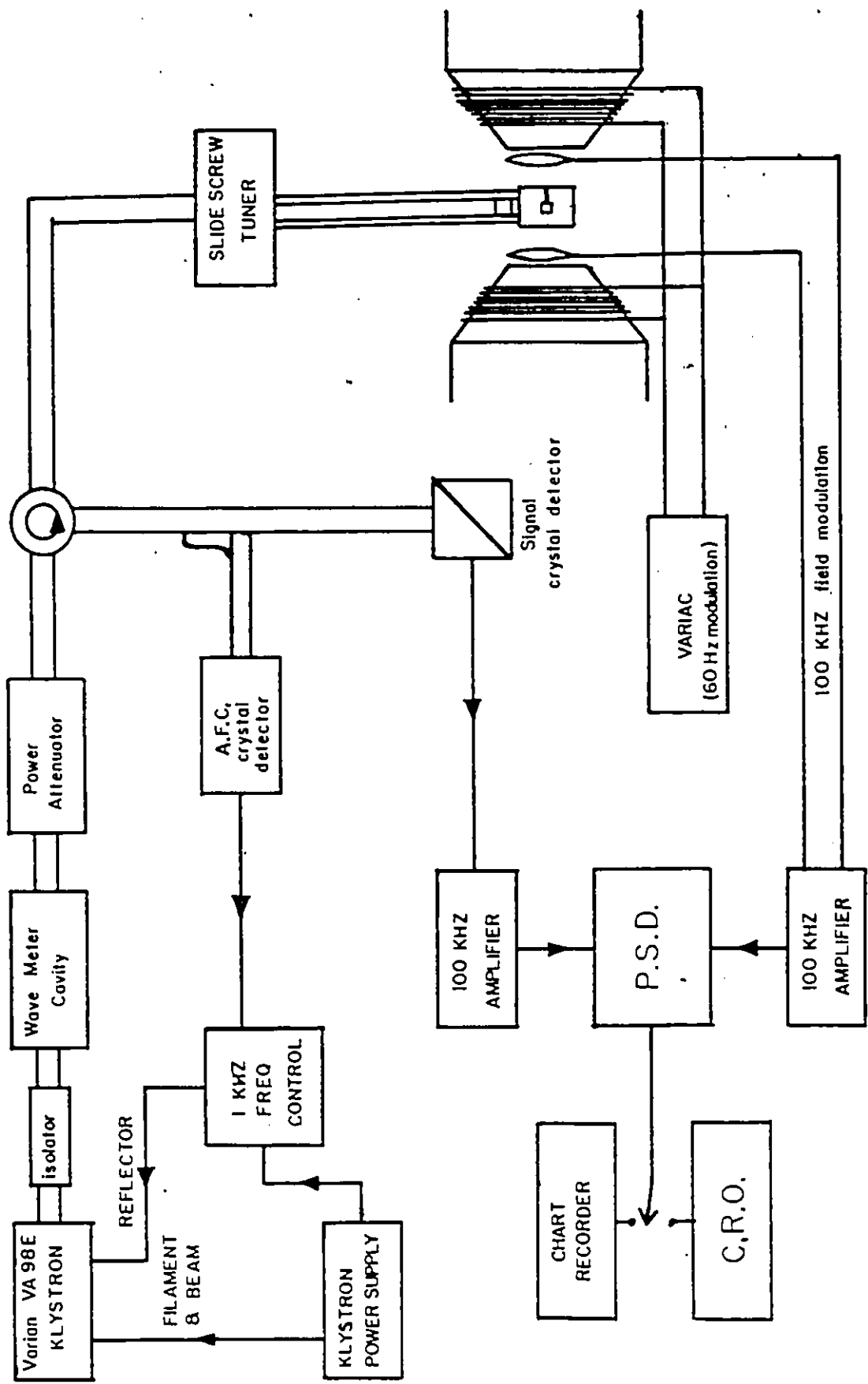


FIG IV.1

of the cavity; thus stabilizing the klystron on the resonant frequency of the cavity.

## (2) Microwave Circuit

Microwaves are prevented from re-entering the klystron by use of an isolator, which is a two terminal pair microwave ferrite device which makes use of the Faraday effect to permit transmission of microwaves in one direction and prevents their transmission in another direction. A tuneable cylindrical cavity is used as a wavemeter, and an attenuator is used to control the power reaching the sample cavity which may be necessary in cases of saturation.

A three port circulator is used to allow transmission of klystron power to the cavity and power reflected at resonance from the cavity to the detector, without power going directly to the detector or any reflected power returning to the klystron arm. The cavity arm can be matched to the klystron arm by means of a slide-screw tuner. Any E.P.R. absorption in the cavity then causes a mismatch, so that power is reflected from the cavity into the detector arm. In practice the cavity is slightly mismatched in order to allow sufficient power to bias the detector crystal.

Fig. IV.3 shows a diagram of the position of the diodes  $D_1$  and  $D_2$  in the detector waveguide and the transformer circuit. The lines show the distribution of E intensity and it can be seen that  $E_1$  and  $E_2$  are in antiphase so that the signals from

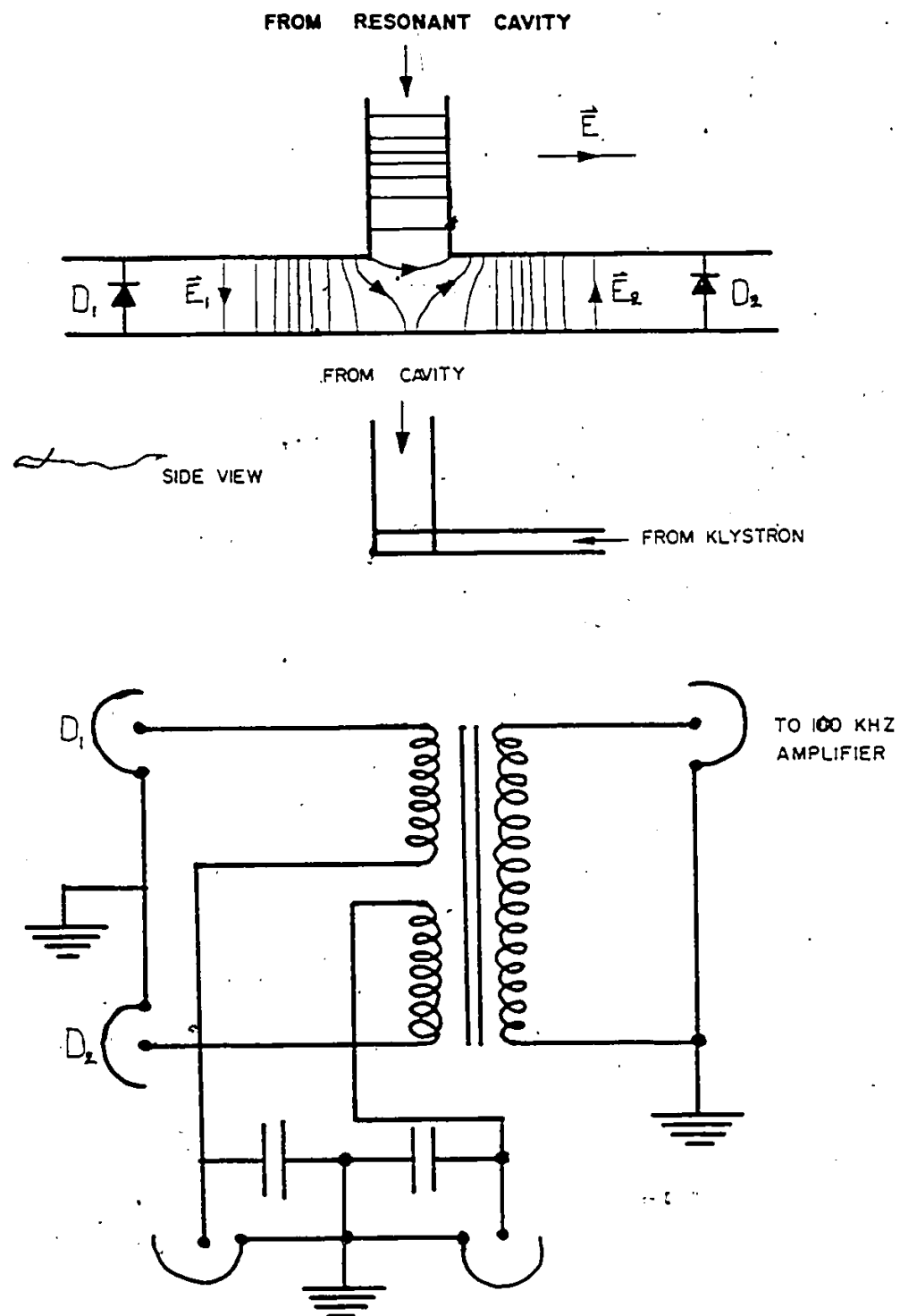


FIG IV.3

$D_1$  and  $D_2$  are also in antiphase.  $D_1$  and  $D_2$  transmit the signal to the 100 KHz amplifier through a transformer with two oppositely directed windings and since noise at  $D_1$  and  $D_2$  is random it will tend to cancel half the time, thus resulting in reduced noise.

The resonant signal is preamplified and then fed into the Princeton Applied Research (P.A.R.) model J.B.-6 lock-in Amplifier, which compare the phase and frequency of the resonant signal with the original 100 KHz modulation signal in the same manner as the P.S.D. of the A.F.C. circuit. The result is a derivative signal proportional to the resonant signal, which can be displayed on the oscilloscope or chart recorder as a function of magnetic field. To facilitate display on the oscilloscope the magnetic field is modulated at 60 Hz with a "Variac", in addition to the 100 KHz modulation. The horizontal sweep of the oscilloscope is connected to a 60 Hz source and synchronised with the modulation using a phase shifter. The method of oscilloscope display allows one to observe E.P.R. signals as both the magnetic field and crystal orientation are varied.

This provides a convenient and rapid means of studying angular variations.

The cylindrical cavity used was made of glass with an internal surface sputtered with gold. Operating in the TE011 mode the cavity has been employed successfully in this laboratory on previous occasions. In conjunction with the cavity is a rotating mechanism previously developed in this laboratory<sup>6</sup>. It facilitates rotation about a horizontal axis which combined with rotation of the magnet about the vertical axis allows an arbitrary orientation of magnetic field.

### (3) External Magnetic Field and Modulation

The external magnetic field is produced by a 12 inch Varian electromagnet with a 3.5 inch gap and a rotating base. The magnet is stabilized by a Fieldial model V-FR 2503 (Varian) control unit, which keeps the field value constant to within one Gauss for several hours. It is possible to achieve a linear sweep of up to 20 KGauss.

Magnetic field modulation at 100 KHz is generated by an oscillator built into the P.A.R. lock in amplifier. This signal is amplified externally and applied to two Helmholtz coils connected in series and mounted on either side of the cavity.

### B. Proton Magnetometer

Measurements of magnetic field strength are obtained by means of a proton magnetic resonance oscillator, tuning circuit and amplifier, together with a wide band amplifier and electronic counter, Hewlett-Packard No. 5253. Several complementary probes using rubber as a proton source were constructed previously in this laboratory to cover a wide frequency range and one probe proved sufficient for all measurements.

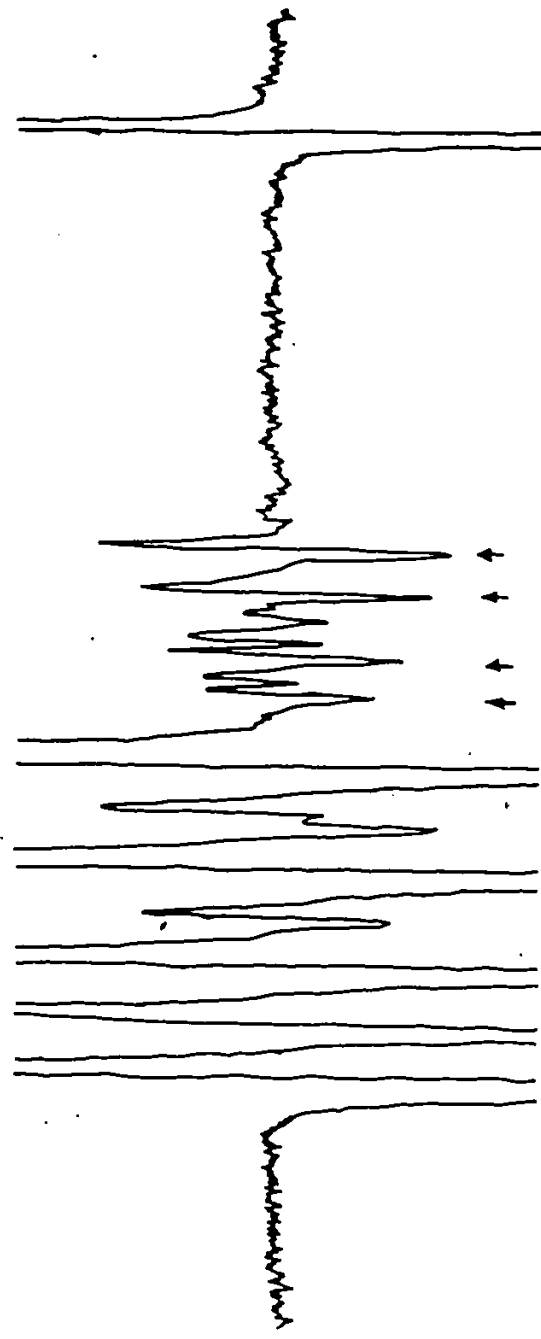
CHAPTER V  
EXPERIMENTAL PROCEDURE

(i) Crystal Orientation

Because the crystals grow preferentially along the b-axis visual examination with the aid of a binocular microscope enabled mounting of the crystals within  $\pm 5^\circ$ . The crystals were attached to the quartz capillaries with epoxy resin and this facilitated placing a thermocouple (copper-constantan) in the capillary in good thermal contact with the crystal for studies of the temperature dependence of the spectra.

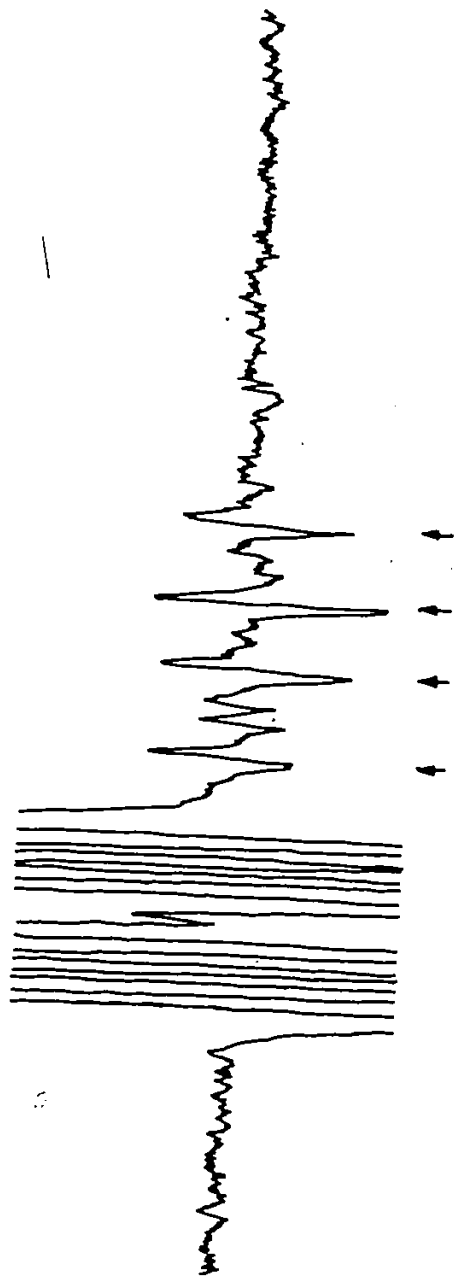
Using the orientation of the magnetic field about a vertical axis and the crystal about a horizontal axis with arbitrary zero the orientations of the magnetic field relative to the crystal were plotted on a stereogram. The accuracy of orientation was checked by recording spectra on a chart recorder at a point where the spectra coincided and then recording the spectra for the magnetic field in the reverse direction; for perfect alignment the spectra should have been identical, in practice deviations of less than  $\pm 0.5^\circ$  were observed. Hence the size of the error bars in the following diagrams.

Diagrams of the spectra in the three crystallographic directions are shown in figs. IV.1-3.



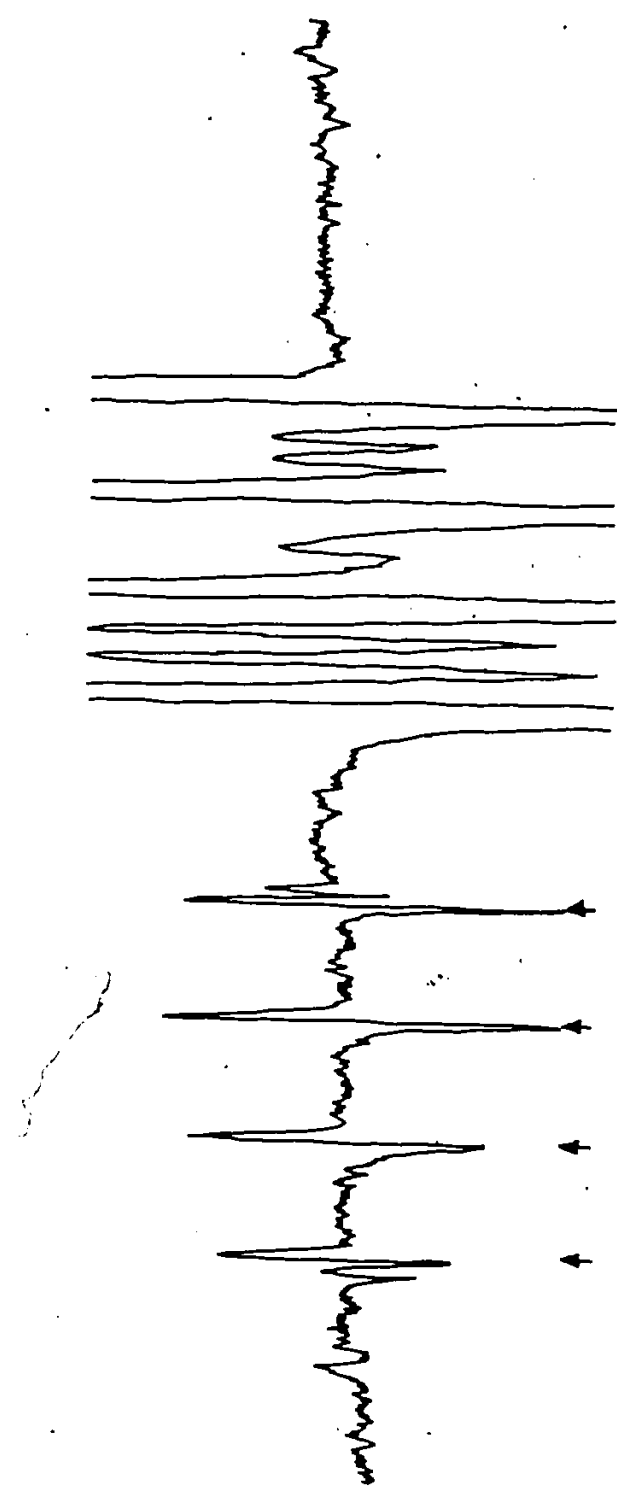
Magnetic field parallel to b

FIG. IV. I



Magnetic field parallel to a

FIG IV.2



Magnetic field parallel to c

FIG IV. 3

The spectra displayed three mutually orthogonal axes coincident with the crystallographic axes at which the three sets of strong lines coincided to form a single set of four lines.

In the planes defined by these axes each set of four lines splits up into two sets of four lines consistent with the unit cell of  $Z=4$  with four sets of crystallographically inequivalent centres for an arbitrary orientation of magnetic field.

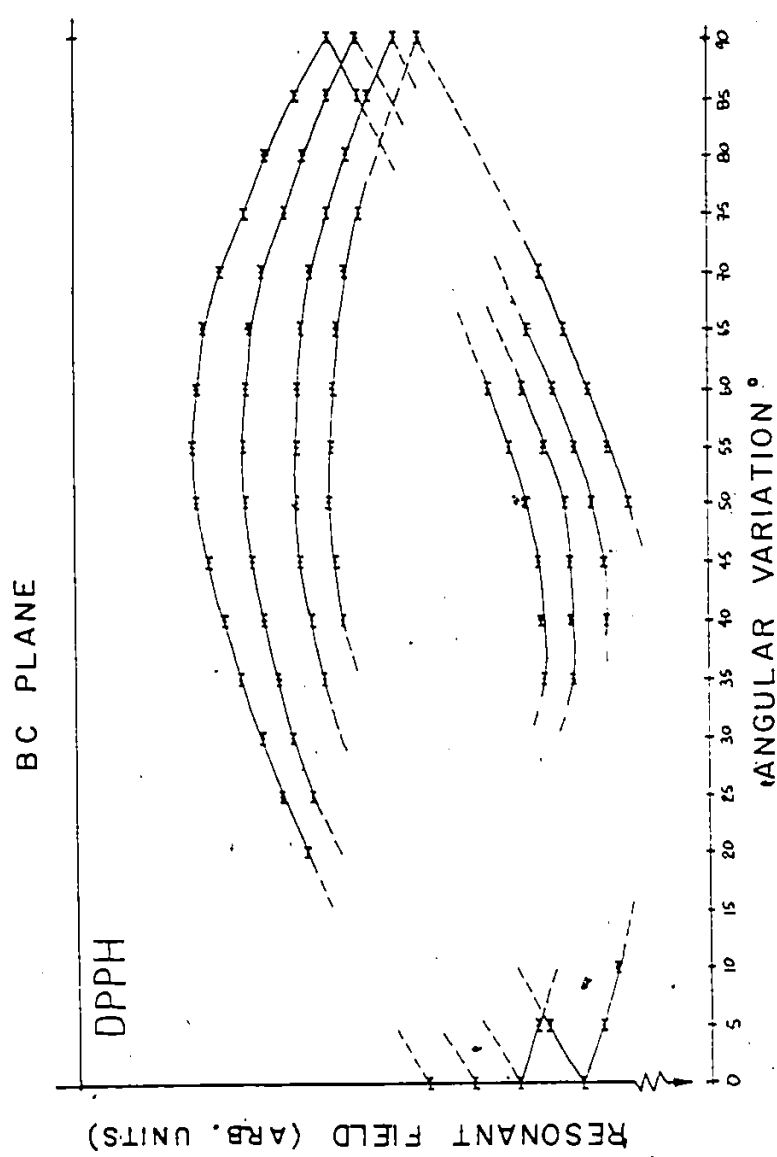
The angular variation of the set of weak lines is shown in figs. IV 4-6 in the ab, bc, ca planes, the gaps occur where the variation was obscured by the set of strong lines.

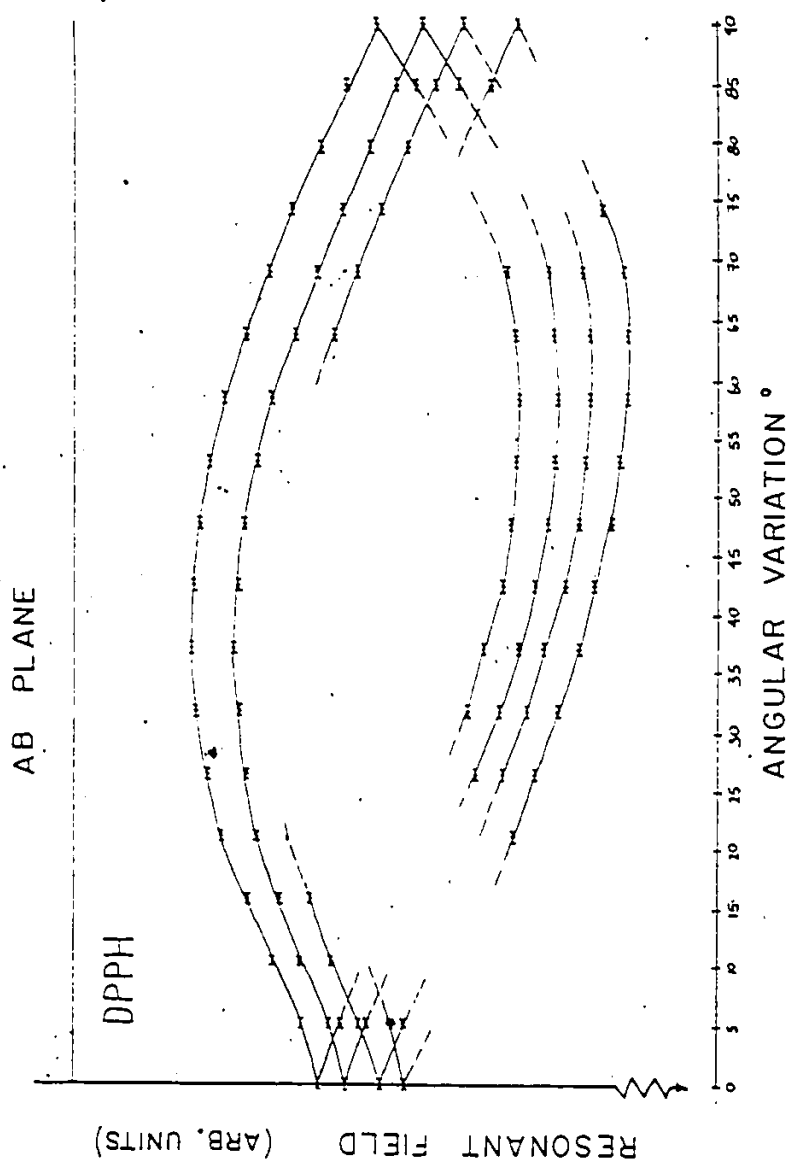
The orientation of the crystallographic axes was confirmed by x-ray analysis (see appendix 2).

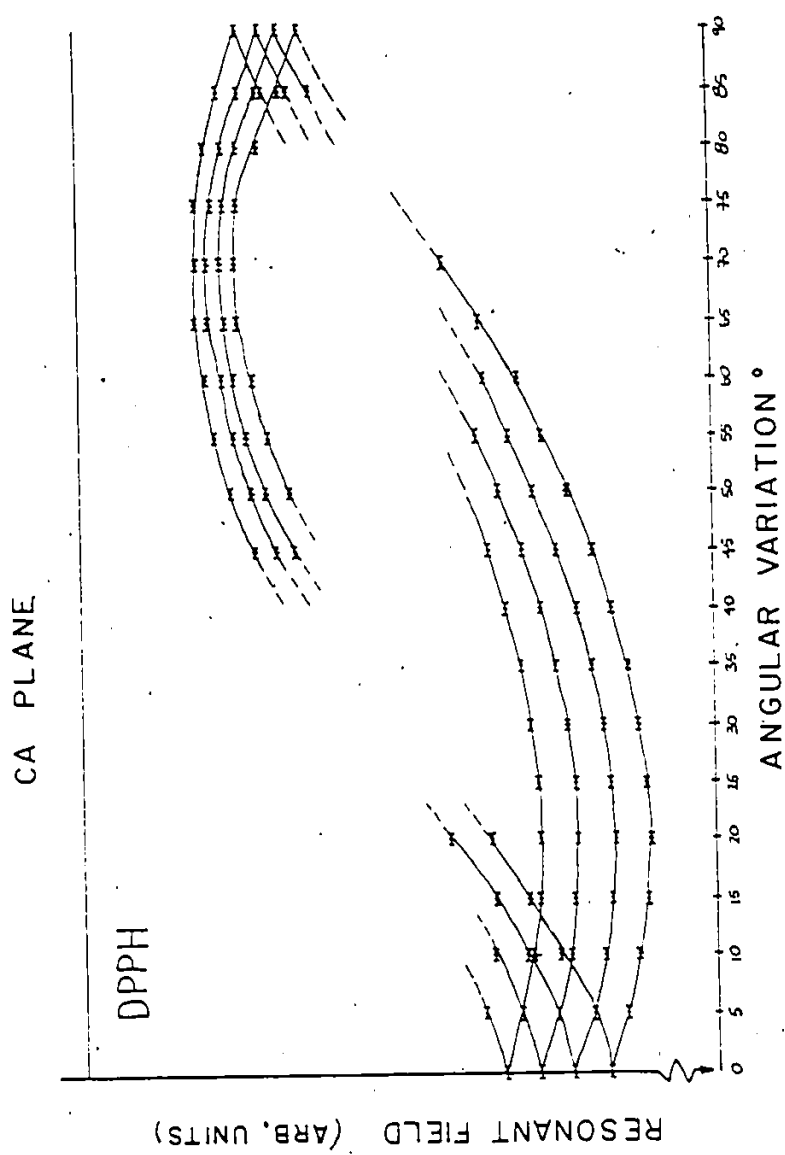
Measurements were taken with a crystal doped with a single isotope Cu<sup>63</sup> and measurements of resonant fields were recorded for 38 orientations, and the directions of magnetic field for a right-handed system of co-ordinates were calculated directly from a plot of all 38 orientations on a stereogram. This allowed for convenient elimination of systematic errors and corrections for misalignment mentioned earlier.

The measurements were taken at orientations a few degrees apart wherever all four lines were not obscured by the stronger ones.

For a batch of crystals grown with Cu<sup>63</sup> ions, many crystals turned out to be twinned, resulting in a complicated addition of spectra and were of no use for this work.







To check that the spectra were in fact due to twinning one crystal was removed from the spectrometer and carefully sliced into two and one half discarded. The spectrum resulting from half the original crystal showed a change of relative intensity of the extra lines with respect to the known set thus confirming their origin as a twinned region of crystal.

The results are tabulated in appendix 1.

### (3) Measurement of Magnetic Field

A set of probes covering the frequency range 30 MHz to 53 MHz had previously been constructed in this laboratory and a single probe proved sufficient for all of our measurements.

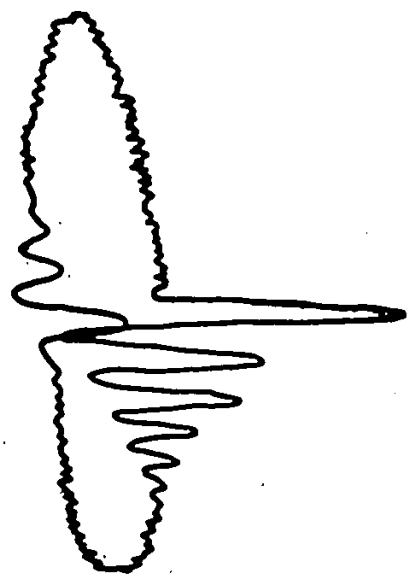
A satisfactory signal intensity was achieved by using a grounded brass tube shielding two stiff wires which carried current to the inductor and which were separated from each other and the shielding by spacers set at intervals along the tube (see fig. V.7).

Actual measurements were made using a double-beam oscilloscope. The crystal rotator and magnet scale were set at the required orientation. Each E.P.R. line in turn was centred on one of the oscilloscope beams, using the second beam the P.M.R. line was tuned to the E.P.R. line. The frequency of oscillation of the P.M.R. signal was then read from the digital output of the electronic counter. This can be converted to a magnetic field strength using the relation

$$\hbar\omega = g_p \beta_N H$$

$$H = \frac{h}{g_p \beta_N} \cdot \omega$$

$$\text{or } H(\text{KGauss}) = 0.234869 \omega(\text{MHz})$$



C.R.O. display of P.M.R. signal.

FIG VI. 8

where;

$H$  is magnetic field strength

$h$  is Planck's constant

$g_p$  is the proton g-value

$\beta_N$  is the nuclear magneton

$\omega$  is the frequency of oscillation

Typical C.R.O. display is shown in fig V.8.

Since the 60 Hz modulation was only 20 Gauss the error in reading C.R.O. scale could not have exceeded 2 Gauss and was thus of no concern as a major source of error.

#### (4) Measurement of Microwave Frequency

A small amount of the free radical D.P.P.H. (diphenyl picryl hydrazyl) was attached to the sample with glycerine and acted as a marker to measure the microwave frequency using the relation

$$\omega = g_{DPPH} H_{DPPH}$$

$$\omega = \frac{g_D \beta}{h} \cdot H_D$$

where;

$\omega$  = microwave frequency

$g_D$  = D.P.P.H. g value = 2.0036

$H_D$  = field value at D.P.P.H. resonance

The D.P.P.H. E.P.R. line is extremely exchange narrowed and gives a very narrow temperature independent line.

## CHAPTER VI

### DEVELOPMENT OF COMPUTER PROGRAM FOR FITTING OF DATA

#### A. The method

A method of parameter fitting using multi-dimensional Newton-Raphson Least-Squares minimization developed by Dr. W. E. Baylis was used so that the program could be generalized. This enabled it to accept data at any orientation and to fit a curve using data from different orientations rather than different frequencies.

The one dimensional Newton-Raphson Method<sup>7</sup> is obtained analytically from the following condition on the Taylor series expansion

$$f(\chi_n + h) = f(\chi_n) + h \cdot f'(\chi_n) + \frac{h^2}{2!} f''(\chi_n) + \dots = 0$$

Where  $\chi_n$  is an approximation of the root of the equation. This can be written in partial derivative form as

$$\frac{\partial}{\partial \chi_n} f(\chi_n + h) = \frac{\partial}{\partial \chi_n} f(\chi_n) + h \cdot \frac{\partial}{\partial \chi_n} f'(\chi_n) + \dots = 0$$

The problem of fitting the experimental data can be overcome in the following way. The Hamiltonian can be expressed as a function of a number of fitting parameters  $p_i$  ( $i = 1, 2, \dots, I_{\max}$ ) and the experimentally measured magnetic field values  $B_1$  and other experimental parameters necessary such as orientation  $K$  or temperature  $T$ .  $B$  is a function of orientation so that the resonant fields occur as  $(N-1)$  values for each of  $M$  orientations.

where  $N$  will represent the degeneracy of the ground state. So the Hamiltonian can be expressed as

$$H = H(P_1, P_2, \dots, P_{I_{\max}}, \vec{B}, \vec{K}, T, \dots) \quad \text{VI.1}$$

The Hamiltonian is represented in an  $n$ -dimensional basis

The matrix elements for the Hamiltonian and its first and second derivatives with respect to the parameters must be known or able to be calculated.

$$\langle \alpha | H | \beta \rangle \quad \text{VI.2}$$

$$\langle \alpha | \frac{\partial H}{\partial p_i} | \beta \rangle \quad \text{VI.3}$$

$$\langle \alpha | \frac{\partial^2 H}{\partial p_i \partial p_j} | \beta \rangle \quad \text{VI.4}$$

The matrix elements of VI.2 and VI.3 for our Hamiltonian are easily calculated knowing the matrix elements of  $I = 3/2$  and  $S = 1/2$  within the manifold of  $\{|\vec{S}\rangle \otimes |\vec{I}\rangle\}$ . As the parameters occur linearly in the Hamiltonian with no cross products the elements of VI.4 will be zero.

For each set of external parameters ( $B, K, T, \dots$ ), (in this case for  $M(N-1)$  resonant field values), the Hamiltonian is diagonalized using the subroutine is basically an extension of the Jacobi method to Hermitean matrices<sup>8,9</sup> and is double precision, complex.

A new set of basis vectors  $\{|i\rangle\}$ , (in terms of the original set  $\{|\alpha\rangle\}$ ,  $|i\rangle = \sum_{\alpha} \langle \alpha | i \rangle$ ) is then obtained in which the Hamiltonian is diagonal

$$\langle i | H | j \rangle = E_i \delta_{ij} \quad \text{VI.5}$$

The difference between one adjacent pair of eigenenergies  $(E_{k_1} - E_{k_2})$  will correspond to the transition energy experimentally

determined from measurement of the microwave frequency  $\omega_k$ . The correspondence between the pair of eigenenergies chosen and the resonant field representing that transition must be known. In this case the correspondence was determined and the programming simplified by taking all measurements at orientations above the resonant lines were clearly observed.

A least squares sum is formed from:

$$f = \{(E_{k_1} - E_{k_2}) - \omega_k\}^2 \quad VI.6$$

$$= \left\{ \left( E_{k_1} - E_{k_2} \right) - \frac{g_D H_D}{g_S} \right\}^2 \quad VI.7$$

where the transition energy in VI.7 is expressed in units of Gauss and is determined from the resonant field of DPPH( $H_D$ ). The value of the least squares sum  $f$  is then determined by summing over the total number of transitions measured  $(N-1)M$  and dividing by the number of degrees of freedom ( $N$  free = number of transitions - number of parameters).

The multi dimensional Newton-Raphson method finds the value of  $P = (p_1, p_2, \dots, p_i)$ , representing a vector in  $i$ -dimensional space where  $i$  is the number of parameters, such that  $\frac{\partial f}{\partial p_i}(p) = 0$  by solving iteratively the equation for the displacement:

$$\frac{\partial f(p + \delta)}{\partial p_i} \approx \frac{\partial f(p)}{\partial p_i} + \sum_j \frac{\partial^2 f(p)}{\partial p_i \partial p_j} \delta_j = 0$$

the solution is:

$$\delta_i = - \sum_j M_{ij} \frac{\partial f(p)}{\partial p_j}$$

VI.8

where  $(M_{ij})$  is the inverse of  $(\frac{\partial^2 f(p)}{\partial p_i \partial p_j})$

and

$$\sum_{Mij} \frac{\partial^2}{\partial p_j \partial p_i} f(p) = \delta_{ii}$$

The inversion is carried out by the subroutine DMINV (see appendix 5). The value of  $\delta_{ii}$  is then added to  $p_i$  to give the new estimate of the parameter.

The first and second derivatives of the least squares sum  $f$  required in the calculation are determined using perturbation theory.

$$\begin{aligned} \frac{\partial f}{\partial p_i} &= \frac{\partial}{\partial p_i} \frac{\sum_k \left\{ (E_{k_1} - E_{k_2}) - \frac{g_D H_D}{g_s} \right\}^2}{N_{\text{free}}} \\ &= 2 \sum_k \left( \frac{\partial E_{k_1}}{\partial p_i} - \frac{\partial E_{k_2}}{\partial p_i} \right) \frac{\left\{ (E_{k_1} - E_{k_2}) - \frac{g_D H_D}{g_s} \right\}}{N_{\text{free}}} \end{aligned} \quad \text{VI.9}$$

and

$$\begin{aligned} \frac{\partial^2 f}{\partial p_i \partial p_j} &= 2 \sum_k \left( \left( \frac{\partial E_{k_1}}{\partial p_i} - \frac{\partial E_{k_2}}{\partial p_i} \right) \left( \frac{\partial E_{k_1}}{\partial p_j} - \frac{\partial E_{k_2}}{\partial p_j} \right) \right. \\ &\quad \left. - \left( \frac{\partial^2 E_{k_1}}{\partial p_i \partial p_j} - \frac{\partial^2 E_{k_2}}{\partial p_i \partial p_j} \right) \frac{\left\{ E_{k_1} - E_{k_2} - \frac{g_D H_D}{g_s} \right\}}{N_{\text{free}}} \right) \end{aligned} \quad \text{VI.10}$$

where

$$\frac{\partial E_k}{\partial p_i} = \lim_{\delta_i \rightarrow 0} \left\{ \frac{E_k(p + \delta_i \hat{i}) - E_k(p)}{\delta_i} \right\}$$

Where  $\hat{i}$  is a unit vector in  $i$ -dimensional parameter space and where  $E_k(p + \delta_i \hat{i})$  is the eigenenergy corresponding to  $E_k(p)$  of the Hamiltonian  $H(p + \delta_i \hat{i})$ , to first order in  $\delta_i$

$$H(p + \delta_i \hat{i}) \approx H(p) + \frac{\partial H(p)}{\partial p_i} \delta_i$$

Using perturbation theory the eigenenergy can also be expressed to first order in  $\delta_i$

$$E_k(\underline{p} + \delta_i \hat{\underline{i}}) = E_k(\underline{p}) + \left\langle \underline{k} \left| \frac{\partial H}{\partial p_i} \right| \underline{k} \right\rangle \delta_i$$

and consequently

$$\frac{\partial E_k}{\partial p_i} = \left\langle \underline{k} \left| \frac{\partial H}{\partial p_i} \right| \underline{k} \right\rangle \quad \text{IV.11}$$

similarly

$$\frac{\partial^2 E}{\partial p_i \partial p_j} = \lim_{\delta_i, \delta_j \rightarrow 0} \frac{E(\underline{p} + \delta_i \hat{\underline{i}} + \delta_j \hat{\underline{j}}) - E(\underline{p} + \delta_i \hat{\underline{i}}) - E(\underline{p} + \delta_j \hat{\underline{j}}) + E(\underline{p})}{\delta_i \delta_j}$$

Now to second order in  $\delta$ 's

$$\begin{aligned} H(\underline{p} = \delta_i \hat{\underline{i}} + \delta_j \hat{\underline{j}}) &= H(\underline{p}) + \frac{\partial H}{\partial p_i} \delta_i + \frac{\partial^2 H}{\partial p_i \partial p_j} \delta_i \delta_j \\ &+ \frac{\partial H}{\partial p_j} \delta_j + \frac{1}{2} \left( \frac{\partial^2 H}{\partial p_i^2} \delta_i^2 + \frac{\partial^2 H}{\partial p_j^2} \delta_j^2 \right) \\ &= H(\underline{p}) + V \end{aligned}$$

where  $V$  may be considered a small perturbation. As the parameters appear linearly in the Hamiltonian the last item goes to zero. By second order perturbation, the eigenenergies are shifted to

$$E(\underline{p} = \delta_i \hat{\underline{i}} + \delta_j \hat{\underline{j}}) = E(\underline{p}) + \left\langle \underline{k} \left| V \right| \underline{k} \right\rangle + \sum_{l \neq k} \frac{\left\langle \underline{k} \left| V \right| \underline{l} \right\rangle \left\langle \underline{l} \left| V \right| \underline{k} \right\rangle}{E_k - E_l}$$

Thus

$$\frac{\partial^2 E}{\partial p_i \partial p_j} = \left\langle \underline{k} \left| \frac{\partial^2 H}{\partial p_i \partial p_j} \right| \underline{k} \right\rangle + i \Re \sum_{l \neq k} \frac{\left\langle \underline{k} \left| \frac{\partial H}{\partial p_i} \right| \underline{l} \right\rangle \left\langle \underline{l} \left| \frac{\partial H}{\partial p_j} \right| \underline{k} \right\rangle}{E_k - E_l}$$

where the matrix elements  $\left\langle \underline{k} \left| M \right| \underline{l} \right\rangle$  written in terms of the old basis are

$$\langle k|M|l \rangle = \sum_{\alpha, \beta} \langle k|\alpha \rangle \langle \alpha|M|\beta \rangle \langle \beta|l \rangle \quad VI.12$$

The similarity transformation is carried out by the subroutine STCM (see appendix 5)

Probable errors are calculated as follows, since  $f$  may have a probable error given by  $\Delta f \approx f/N_{\text{free}}$  the corresponding  $\sigma_i$  in  $\pi_i$  is given by

$$\Delta f \approx \sqrt{\sum_{ij} M_{ij} \sigma_i \sigma_j} \approx f / N_{\text{free}}$$

The values of  $\sigma_i^2$  are calculated from inversion of the above giving,

$$\sigma_i^2 = 2M_{ii}^{-1} (f/N_{\text{free}})$$

#### B. The flow chart

From the flow chart (see fig. VI.1) the steps in the computational process can be followed.

1. The data is read in including all external parameters, initial estimates of the crystal parameters and the matrix elements of operators required in the equivalent Hamiltonian. The input data after conversion is printed out.
2. The matrix elements that are independent of the field are calculated.
3. The remaining field dependent matrix elements are calculated using the components of the measured field values in addition to data utilised in 2. (see appendix 6 for RTN1)

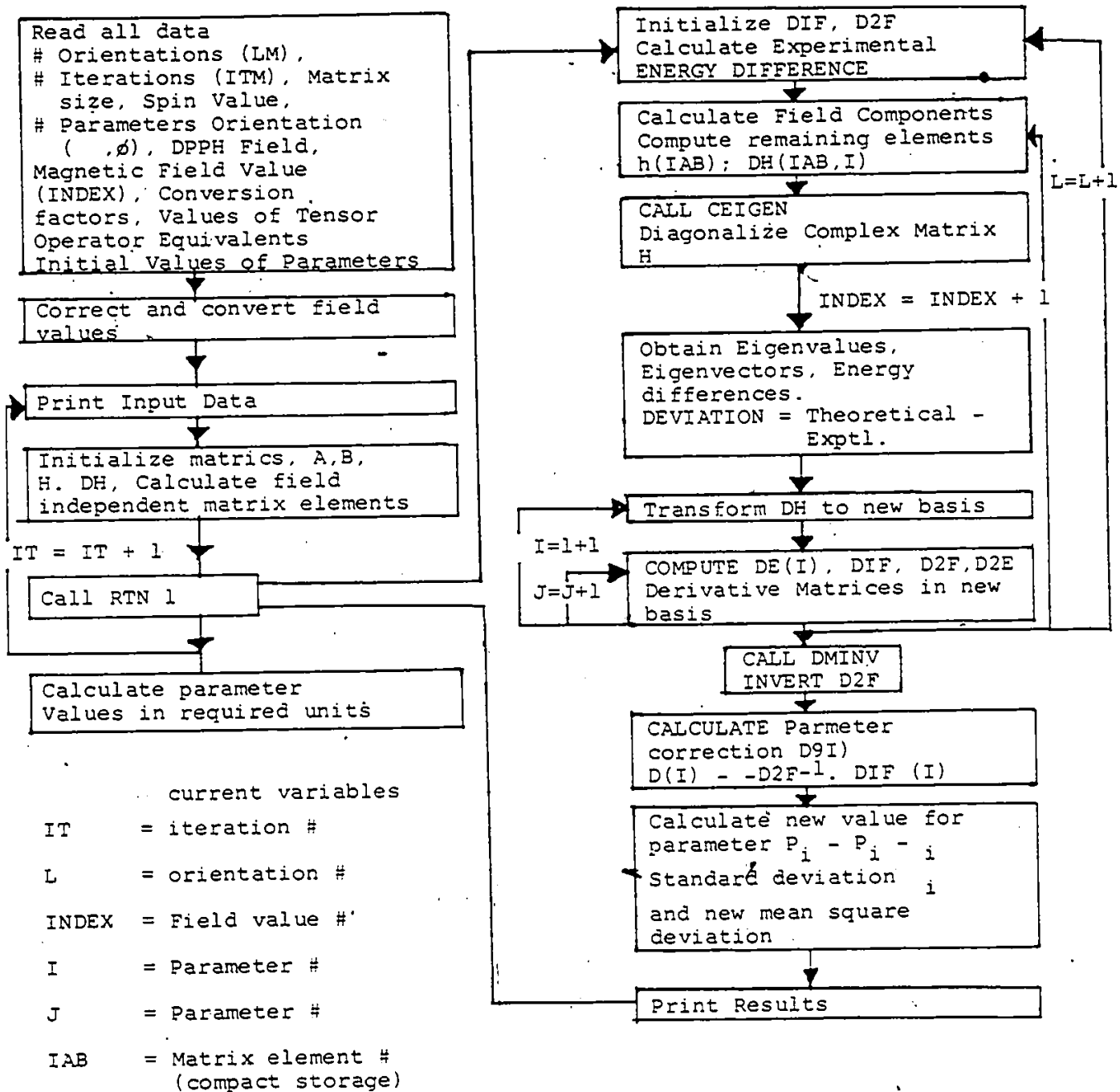


Fig. VI.1. FLOW CHART FOR COMPUTER PROGRAMME

4. The Hamiltonian matrix form in 2 and 3 is then diagonalized exactly using the subroutine CEIGEN (see appendix 7) which returns eigenenergies and eigenvectors. The difference between the adjacent eigenvalues provides the basis of the least squares sum while the eigenvectors are used in the similarity transformation in the next step. The value of DEVIATION printed out is a measure of the fit.
5. The derivative matrix is then transformed to the new basis in which the Hamiltonian is diagonal, see (VI.12). This then allows calculation of DE(I), the derivative of the energy with respect to each parameter, see (VI.11). From these the first and second derivatives of the least squares fit are formed, D1F(I), see VI.9, and D2F(I), see VI.10.  
Step 5 is repeated for each parameter in the  $I = I + 1$  loop, while the computation of the second derivative is repeated for all parameters J, with each parameter I in the  $J = J + 1$  loop.  
Steps 3 - 5 are then repeated for each of the  $(N - 1)$  resonant fields at a given orientation during the  $INDEX = INDEX + 1$  loop, which itself is repeated for all of the orientations in the  $L = L + 1$  loop.
6. As D2F involves summation of both I & J simultaneously as well as a summation over all of the resonant fields, it is not completed until the end of step 5. D2F is then inverted using DMINV (see appendix 7). The parameter connection D(I) can then be calculated see VI.8,

the new estimate of the parameters is then determined

$$P(I) = P(I) + D(I)$$

The standard deviation for each parameter is then calculated together with an estimate of what the mean square deviation will be, using the new parameter values.

7. The results are printed and control returned to the main program where steps 2 to 7 are repeated for the number of iterations specified.
8. The parameters are converted to whatever units are required and any auxiliary calculations with the parameters may also be carried out here.

As a check on the inversion process and the reliability of the parameter values, the  $D^2F$  and  $(D^2F)^7$  matrices are multiplied using the subroutine DGMPRO (see appendix 8), based on IBM routine GMPROD)<sup>10</sup> to see that the product is the unit matrix. (see VI.8)

#### C. Rate of Convergence

To indicate the rate of convergence a sample run is shown in table VI.1 giving the mean square deviation in KGauss.

TABLE VI.1

Iteration Number	Mean Square Deviation (KGauss) <sup>2</sup>
1	0.9190
2	0.0220
3	0.0550
4	0.0022
5	0.0200
6	0.0006

Even though the values oscillates it can be seen that convergence is quite rapid.

## CHAPTER VII

### DISCUSSION AND CONCLUSION

In total thirty eight orientations were used to collect data; with orientations in all three planes included. For the fitting of parameters in the spin Hamiltonian nineteen were rejected because they gave for larger deviations from the trial energy levels than the remaining twenty nine. In excess of a dozen iterations were needed before an acceptable fit was obtained and from then on the quality deteriorated.

The best fit parameters are tabulated in table VII.1. The results are presented in the co-ordinate system discussed previously.

These results will be discussed in the light of previous reports, Abdulsabirov<sup>1</sup> had investigated the three strong sets of lines and had fitted data to an orthothom bic spin Hamiltonian,

$$H = \vec{H} \cdot \vec{g} \cdot \vec{S} + \vec{S} \cdot \vec{A} \cdot \vec{I}$$

in which the g and A "tensor" shared common principal axes. They found that the orientations of these three sets axes were completely different and correlated these orientations with the crystallography with the help of X-ray analysis.

TABLE VII.1

g values

$g_{xx}$	$g_{yy}$	$g_{zz}$
$2.5396 \pm .0001$	$2.1296 \pm .0002$	$2.0920 \pm .0001$
$g_{xy}$	$g_{zx}$	$g_{zy}$
$0.1023 \pm .0001$	$0.0347 \pm .0001$	$0.0516 \pm .0002$

A values ( $\times 10^{-4} \text{ cm}^{-1}$ )

$A_{xx}$	$A_{yy}$	$A_{zz}$
$205.3 \pm 0.9$	$19.9 \pm 5.6$	$38.5 \pm 4.0$
$A_{xy}$	$A_{zx}$	$A_{zy}$
$88.3 \pm 2.0$	$2.3 \pm 1.6$	$-36.9 \pm 4.5$

Q values ( $\times 10^{-4} \text{ cm}^{-1}$ )

$Q_x$	$Q_y$
$20.6 \pm 2.0$	$3.8 \pm 0.6$

N.B.: Above expressed in crystallographic coordinate system described earlier.

Since  $\text{Cu}^{2+}$  is doubly charged, it substitutes for  $\text{K}^{1+}$  in the lattice of  $\text{K}_2\text{SO}_4$  overall electrical neutrality can only be preserved if some kind of charge compensation occurs. Abdulsebirov<sup>1</sup> proposed that this compensation occurs via a vacancy on an adjacent  $\text{K}^{1+}$  site. A diagram of the crystal structure of  $\text{K}_2\text{SO}_4$  projected along the c-axis is shown in fig. VII.1. The  $\text{K}_1$  and  $\text{K}_2$  sites differ in environment but the four of which occur in each

unit cell are related by the symmetry of the crystal. If the  $\text{Cu}^{2+}$  impurity substitutes for a  $\text{K}^{1+}$  as proposed by Abdulsabirov<sup>1</sup> then a vacancy on an adjacent  $\text{K}^{1+}$  site will strongly influence the g tensor and will rotate on principal axis towards the direction joining the  $\text{Cu}^{2+}$  impurity and the vacancy. Abdulsabirov<sup>1</sup> found that the above is consistent with  $\text{Cu}^{2+}$  substituting for  $\text{K}^{1+}$  on a  $\text{K}_2$  type site with a vacancy on an adjacent  $\text{K}_1$  type site. They found that the principal axis of the g tensor (ie. largest principal value) for the three centre types was within a few degrees of the line joining the  $\text{K}_1$  and  $\text{K}_2$  type positions. These  $\text{K}_2^+ - \text{K}_1^+$  directions are marked 1,2,3 on fig. VII.1. They also mention the fourth weak set of lines investigated here and suggest that they may be due to a centre produced when charge compensation occurs on the fourth adjacent  $\text{K}_1^+$  site. The line joining  $\text{K}_2^+$  to this fourth adjacent site drawn and labelled 4 in fig. VII.1. The directions of the principal values of the g tensor observed by Abdulsabirov<sup>1</sup> are inconsistent with  $\text{Cu}^{2+}$  substituting on a  $\text{K}_1$  type site and charge compensation occurring on a  $\text{K}_2$  type site as can easily be verified. Why substitution should occur on  $\text{K}_2$  and not  $\text{K}_1$  type sites is not known but it can be noted that  $\text{K}_1$  type sites have an oxygen much closer than  $\text{K}_2$  type sites.

Our results are in fair agreement with the above as follows. The fitted parameters in table VII.1 indicate that the g "tensor" can be adequately fitted by a symmetric tensor and the A "tensor" not so adequately although as can be seen any observed asymmetry in A is slight.

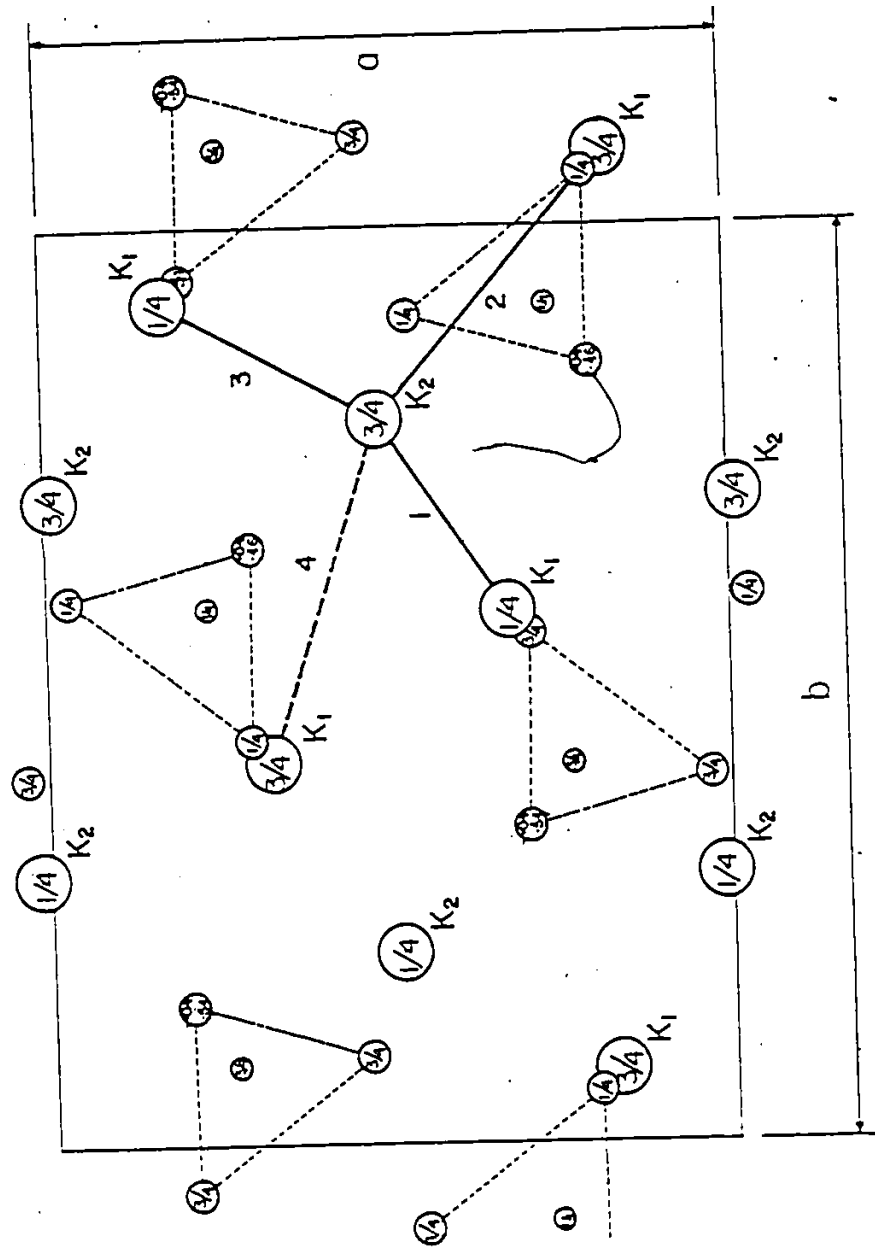
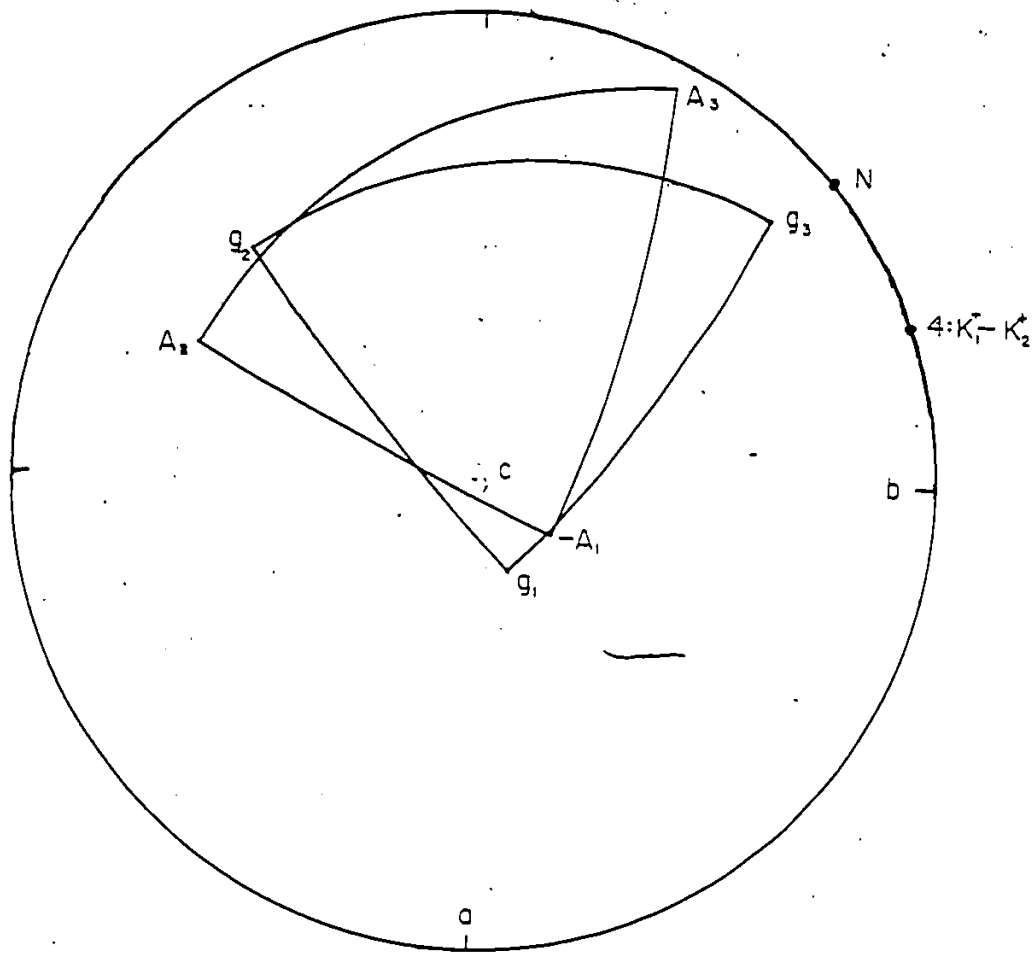


FIG VII. I



Stereogram of principal axes of  $g$  and  $A$  tensors  
with respect to crystallographic axes ,

FIG VII.2

It is generally agreed that  $g$  is symmetric in the absence of an external electric field. If we assume that the  $g$  and  $A$  "tensor" can be adequately fitted by symmetric sets of parameters then  $g$  and  $A$  can be diagonalized (see appendix 10 for method) to yield the principal axes. These are shown on a stereogram in fig. VII.2 and the principal values tabulated in table VII.2 below. On the stereogram the principal directions of the  $g$  and  $A$  "tensors" are displayed as points joined by lines of  $90^\circ$ . The stereographic axes are those of the crystal and the line labelled 4 in fig. VII.1 is shown in the ab plane.

TABLE VII.2

$g_1$	2.122	$A_1$	55.3
$g_2$	2.052	$A_2$	-32.9
$g_3$	2.407	$A_3$	241.3
$(\times 10^{-4} \text{ cm}^{-1})$			

As pointed out by Abragam and Bleaney<sup>11</sup>  $g$  and  $A$  are not time second rank tensors, rather  $gg$  and  $AA$ , however since we are taking both  $g$  and  $A$  to be symmetric diagonalizing  $g$  necessarily diagonalizes  $gg$  etc., and so the principal axes and values are unchanged.

As can be seen from the stereogram clear non coincidences in  $g$  and  $A$  principal axes are observed particularly for  $g_3$  and  $A_3$ . Fair corroboration of Abdulsavirov<sup>1</sup> can be seen with an angle of  $22^\circ$  between direction  $K_2^+ - K_1^+$  : 4 and  $g_3$ . Even more significant is the fact that  $g_3$  is within  $9^\circ$  of the nor-

mal to the rectangle formed by the remaining  $K_1$  ligands nearest the vacancy. This is labelled N on the stereogram.

Freeman and Dilbrow<sup>2</sup> have also investigated  $K_2SO_4:Cu^{2+}$  and isostructural  $Rb_2SO_4:Cu^{2+}$  and have reported not only noncoincidences in g and A principal axes of  $8^\circ$  but also asymmetrics in A. They also cite five other recently reported cases of low symmetry. They only concentrated on centre type 1 as defined by Abdulsabirov<sup>1</sup> (direction 1 and fig. VII.1) and omitted a quadrupole term. However for our set of weak lines  $M_I = \pm 1$  transitions varies greatly with direction.

Non-coincidence of g and A tensor is allowed whenever the point symmetry at a paramagnetic ion is monoclinic or triclinic but not for higher symmetrics. As fig. VII.2 shows we are clearly dealing here with a case of triclinic symmetry, since non-coincidences in excess of  $12^\circ$  for all axes are clearly demonstrated and there is no common principal axis which would result from monoclinic ( $C_2$ ) or higher symmetry<sup>12</sup>.

As discussed by Belford et al<sup>12</sup>, for such low symmetry the A tensor need not be symmetric but the limitation with orientation dependent measurements on single crystals is that  $A_x$ ,  $A_y$  and  $A_z$  (XYZ being the principal axis system of the A tensor) along with two Euler angles parameterizing the disposition of gg and AA can be measured, but A has nine independent components so that A cannot be completely characterized. In practical terms this means that even if A is genuinely asymmetric it may not be possible to detect asymmetrics.

On a molecular level the problem of the ground state may be very crudely approached by 1st order perturbation theory. It can be shown that a cubic environment with a tetragonal elongation produces the energy level scheme shown below in fig. VII.3.

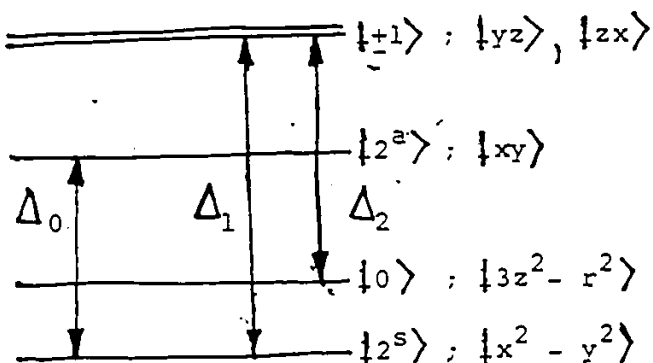


fig. VII.3

Spin orbit coupling cannot mix  $|3z^2 - r^2\rangle$  and  $|x^2 - y^2\rangle$  but mixes in some of the  $|zx\rangle$  and  $|xy\rangle$  to give an axial g tensor

$$g_{11} = 2 - \frac{8\lambda}{\Delta_0}$$

$$g_1 = 2 - \frac{2\lambda}{\Delta_1}$$

This is in contrast to a  $|3z^2 - r^2\rangle$  ground state which gives

$$g_{11} = 2$$

$$g_1 = 2 - \frac{6\lambda}{\Delta_2}$$

This shows that we are dealing with a predominantly square-planar ground state ie.  $|x^2 - y^2\rangle$  in the plane formed by the four coordinating  $K_+$  sites with the normal N.A low symmetry crystal field however may mix  $|x^2 - y^2\rangle$  with  $|3z^2 - r^2\rangle$  and

the g values observed can be fitted to a 1st order perturbation expression to give a ground state.

$$|g\rangle = \alpha(|x^2 - y^2\rangle + \beta|3z^2 - r^2\rangle)$$

with  $\beta = 0.065$

In other words the effect of the vacancy is to mix in  $|3z^2 - r^2\rangle$  with z pointing towards the vacancy.

Presumably this centre occurs less frequently for energetic reasons and since the signal is proportional to the concentration of paramagnetic centres this allows a rough estimate of the relative occurrence of the different centre types. This yields an occurrence rate 0.3% that of the other centres which have signals of roughly equal strength.

At any rate the concluding remarks to be made from this investigation are to tentatively confirm the hypothesis of Abdulsabirov<sup>1</sup> and to report a case of Cu<sup>2+</sup> occupying a low symmetry site resulting in non-coincidences in excess of 12° in gg and AA principal axes.

## BIBLIOGRAPHY

1. Abdulsabirov, R.Y., Greznev, Yu. S. and Zeripov, M.M., Soviet Physics - solid State, Vol. 12. No. 2 Aug. 1970.
2. Freeman, T.E. and Pilbrow, J.R., J. Phys-C: Solid State Vol. 7, 1974.
3. Robinson, F.M.T., J. Phys, Che., 62, 925-928.
4. Zarayskiy, Ye.K.Zh., EKsp. Teor. Fiz 17, 155, 1947.
5. Griffith, J.S., "The Theory of Transition Metal Ions," Cambridge Univ. Press, 1961.
6. Holuj, F., Can. J. Phys. 46, 287 1968.
7. Froberg, C.E., "Introduction to Numerical Analysis", Addison-Wesley.
8. Ibid., p 111.
9. I.B.M. publication 360A-CM, p 165.
10. Ibid., p 95.
11. Abragam, A. and Bleaney, B., "Electron Paramagnetic Resonance of Transition Ions", Oxford: Clarendon, 1970.
12. Belford, R.L. and Pilbrow, J.R., J. of Mag Res 11, 381-387, 1973.

## APPENDIX 1

## RESULTS

A right-handed coordinate system was chosen which coincided with the crystallographic axes for tabulation of results and input into the parameter fitting program. Polar coordinates were employed and the correspondence is shown below:

$\phi$  azimuthal angle

$\theta$  polar angle

$\phi$	$\theta$	crystallographic axis
0°	0°	b
0°	90°	c
90°	90°	a

Computer printout of results is shown overleaf and the format is as follows

columns 1-4:  $\phi$

columns 5-8:  $\theta$

columns 9-14:  $\omega_{DPPH}$  MHZ

columns 15-20: transition IF = 1 to JF = 8 MHZ

columns 21-26: transition IF = 2 to JF = 7 MHZ

columns 27-32: transition IF = 3 to JF = 6 MHZ

columns 33-38: transition IF = 4 to JF = 5 MHZ

\* A.J.CF 82/0-137 ±

0.00 DEBT OUT OF 5 120.00 ALLEGED

120.00 ALLOCATED

3.00 USED 301 C  
3.00 USED 302 C

120.00 RECORDED  
6 CLASS "A" 11"

更多資訊請參閱《中華人民共和國憲法》、《中華人民共和國立法法》、《中華人民共和國行政許可法》、《中華人民共和國行政處罰法》、《中華人民共和國行政審查法》、《中華人民共和國行政應訴法》等法律。

50.

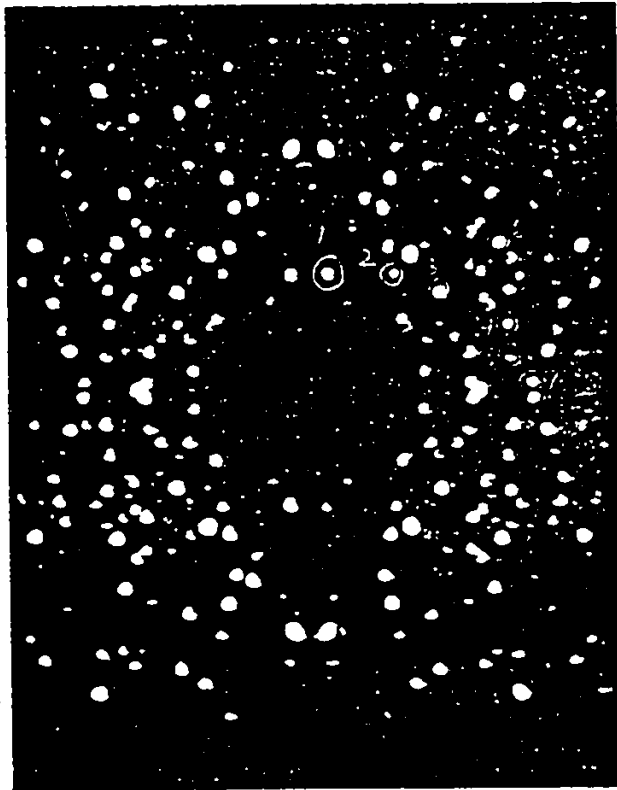
LIST

0000032533366548710054798683702245178869  
00001008832210071653364218275624886894  
0000308743744101274562870511137545264547  
00000441501223674254635642147756022537  
00000577263211874112365700133564740026  
0000052201356547844102236501151430137532  
000014635420310546177001174461723116  
000002473865421038699795204157326557254  
000015335675840219636523475320184863  
0000020135520121257899530215456382778505  
00001599362012225048709532105472623662  
0400040386100751003821374002213799003  
0900134436101054573100086302143862757314  
090003200532103117600164310368768406652  
0900273756521177481173213738407234817  
0900150353012668754210895887046175324  
04970900321054467932015466672214987063  
1303090034210376792363014550755661490682  
04466900342120845312735664000235817334  
1354040103047932101201742150030032017701  
0158009030352104277301142150030032017701  
1614091035210774793012753710002024873641  
315308103821147930120172270480102571403  
164400703521056877510432398510495727522  
012509003521036859752113045667753251319  
26750007033452641070053263496537365286541  
007509003532103659283702014258679532401  
17250007022502104473251016003297111451  
00251907310107400701275600629701133186  
1775000703352101770030030215379543257001  
0000040020144603664648973002134773664  
0000074735200148975245103036455792411231  
0000105735244579011235740213699575324  
000006753285542130063927413589205374192

## APPENDIX 2

## IDENTIFICATION OF CRYSTALLOGRAPHIC AXES

X-ray measurements were performed by Dr. M. Khan with the aid of his four circle diffractometer enabling identification of crystallographic axes. The diffractometer used the Syntex system. A photograph of forward scattering spots produced by the sample crystal is shown below.



## APPENDIX 3

IV G LEVEL 21

MAIN

DATE = 81181

17/50/01

```

C          HAMF  40
C          HAMF 130
C          HAMF 140
C
C      IMPLICIT REAL*8(A-H,C-Z)
C      COMPLEX*16 DCONJG,OH(36:14),DHT(36,14),EVECT(64 ),H(36 ),IMAG,ZERC
1,CA(36),DDP(36),B(36)          HAMF 200
C      DIMENSION A(6),             D1F(14),D2F(196),D2FINV(196),EN( 8),
1 ALPHA(50),BETA(50),D(14), SIGMA(14),HO(50),IF(11),JF(11),F(12),
2 GNAME(2),DE( 14),HDP(50),HEADER(7),P(14),HB(50,11)
2 DATA C1,C2/*GAUSS*/,'10-4CM-1'/.IMAG/(0.00,0.00)/,ZEP0/(0.00,0.00)/HAMF 160
C
C      INPUT FORMAT STATEMENTS
C
100 FORMAT(2I2,F6.1)          HAMF 210
101 FORMAT(2F5.1,3F10.7,2F10.3) HAMF 220
102 FCFMAT(I2,F5.1,I2/7A8,2A8) HAMF 230
103 FCFMAT(8F10.5)          HAMF 240
104 FORMAT(16F5.1)          HAMF 250
105 FCFMAT(8F10.7)          HAMF 260
106 FCFMAT(3F10.7)          HAMF 270
107 FCFMAT(5F10.5)          HAMF 280
110 FORMAT(4(8F10.6/),7F10.6/,2(SF10.6/),2F10.6) HAMF 290
111 FCFMAT(1X,12G10.3)        HAMF 300
C
C      OUTPUT FORMAT STATEMENTS
C
150 FORMAT(1H1,//25X,7A8,2A8) HAMF 310
152 FCFMAT(//1X,'NUMBER OF ORIENTATIONS=',I2,5X,'NUMBER OF ITERATIONSHAMF 320
1=I',I2,5X,'TEMPERATURE(C)=' ,F6.1) HAMF 330
154 FCFMAT(/1X,'SIZE OF MATRIX=',I2,5X,'SPIN VALUE=' ,F6.1,5X,'NUMBER HAMF 340
10F PARAMETERS=' ,I2) HAMF 350
156 FCFMAT(/1X,'DPPH(MHZ)' ,12F9.4) HAMF 360
158 FCFMAT(/1X,'THETA:' ,2X,I2(F7.1,2X)) HAMF 370
160 FCFMAT(/1X,'PHI:' ,2X,I2(F7.1,2X)) HAMF 380
162 FCFMAT(/45X,'*** SPECTRA(MHZ) ***') HAMF 390
164 FCFMAT(/10X,I2(2X,F7.4)) HAMF 400
166 FCFMAT(/1X,I2(F7.3,15X,'DPPH G VALUE=' ,F8.6,HAMF 410
1/,1X,'FREE ELECTRNL MHZ TO GAUSS=' ,F7.3,15X,'DPPH G VALUE=' ,F8.6) HAMF 420
168 FCFMAT(1H1,//50X,'ITERATION #' ,I1///) HAMF 430
169 FCFMAT(14X,'GX' ,10X,'GY' ,10X,'GZ' ,10X,'GXY' ,9X,'GZX' ,9X,'GZY') HAMF 440
170 FCFMAT(14X,'AX' ,10X,'AY' ,10X,'AZ' ,10X,'AXY' ,9X,'AZX' ,9X,'AZY') HAMF 450
171 FCFMAT(14X,'QX' ,10X,'CY' ,10X,'QZ' ,10X,'QXY' ,9X,'QZX' ,9X,'QZY') HAMF 460
172 FCFMAT(1CX,6(2X,F10.5)/) HAMF 470
174 FCFMAT(//1X,5X,'THETA=' ,F6.1,5X,'PHI=' ,F6.1,1//) HAMF 480
176 FCFMAT(23X,'TRANSITION' ,9X,'DEVIATION(GAUSS)') HAMF 490
178 FCFMAT(20X,I2,'/2',2X,'--',2X,I2,'/2',10X,G10.3) HAMF 500
180 FCFMAT(/50X,'PREDICTED DISPLACEMENTS' /,6X,'D(1)',6X,'D(2)',6X,'D(3)',6X,'D(4)',6X,'D(5)',6X,'D(6)',6X,'D(7)',6X,'D(8)',6X,'D(9)',36X,'D(10)',5X,'D(11)',5X,'D(12)') HAMF 510
181 FCFMAT(2X,12F10.5)          HAMF 520
182 FCFMAT(6X,'D(13)',6X,'C(14)',6X,'D(15)',6X,'D(16)',6X,'D(17)',6X,'D(18)') HAMF 530
184 FCFMAT(/50X,'NEW VALUES FOR PARAMETERS') HAMF 540
186 FCFMAT(/50X,'STANDARD DEVIATION FOR EACH PARAMETER') HAMF 550
188 FCFMAT(10X,'VALUE OF' ,I2,'THE PARAMETER IS NOT CONVERGENT') HAMF 560
190 FCFMAT(/5X,'RMS DEVIATION=' ,F8.1,' GAUSS',10X,'NEW RMS DEVIATION=' ,F8.1,' GAUSS',10X,'NUMBER OF LINES=' ,I3) HAMF 570
C
C      READ INPUT DATA CARDS
C
1000 CCNTINUE          HAMF 580
1000 READ 100,LN,ITM,TEMP          HAMF 590
1000 READ 102,N,SPIN,IMAX,HEADER,GNAME          HAMF 600
1000 READ 108,PMHG,GDP,GFE          HAMF 610
1000 READ 106,(P(I),I=1,6)
1000 READ 106,(P(I),I=7,IMAX)
1000 READ 100, NCORE
1000 READ 1011,(IF(K),JF(K),K=1,11)
1011 FCFMAT(12(IX,2I1))
1011 PRINT 162
1011 IN=0
10 IN=IN+1
10 CC 199,K=1,12
199 F(K)=0.0
199 READ 1030,ALPHA(IN),BETA(IN),HO(IN),(F(K),K=1,10)
1030 FFORMAT(6X,2F4.1,12F6.4)
1030 IF(HO(IN).EQ.0.)GOTC30
1030 DC 20 K=1,11
1030 II=IF(K)

```

V G LEVEL 21

MAIN

DATE = 81181

17/50/01

```

JJ=JF(K)
20 HB(IN,K)=F(K)*P4HG
HDP(IN)=HC(IN)*PMHG*GDF/GFE
PRINT 2005,IN,ALPHA(IN),BETA(IN),HO(IN),(IF(K),JF(K),F(K),K=1.8)
2005 FFORMAT('0',2X,I3.2F6.1,F7.4+2X,1I(2I1.1X,F7.4))
GO TO 10
30 LM=IN-1          HAMF 790
                  HAMF 800
                  HAMF 810
                  HAMF 820
                  HAMF 830
                  HAMF 840
C               PRINT INPUT DATA
C
C               PRINT 150,HEADER,GNAME
C               PRINT 152,LM,ITM,TEMP
C               PRINT 154,N,SPIN,IMAX
C               PRINT 166,P4HG,GDF,GFE
C
C               DEFINITIONS
C
C               DR2=DESCFT(2.00)
C               IMAX2=IMAX*IMAX
C               NM=(N+1)*N/2          HAMF 920
C
C               CORRECT AND CONVERT FIELD VALUES
C
C               ITERATIONS LOOP STARTS HERE
C
C               DC 204 IT=1,ITM
C               NL=0          HAMF 930
C
C               INITIALIZATION
C
C               XLSF=0.00
C               DC 207 IJ=1,NM          HAMF 940
C               F(IJ)=ZEOF
C               E(IJ)=ZEOF
C               CA(IJ)=ZERO
C               DDF(IJ)=ZERC
C               DO 207 J=1,IMAX
C               DH(IJ,J)=ZERO          HAMF 950
C               207 DHT(IJ,J)=ZERO      HAMF 960
C               DO 206 IJ=1,IMAX2      HAMF 970
C               206 D2F(IJ)=0.00        HAMF 980
C               DC 208 I=1,IMAX
C               208 D1F(I)=C.D0        HAMF 99
C               PRINT 168,IT
C               PRINT 169
C               PRINT 172,(P(I),I=1,6)   HAMF 1000
C               PRINT 170
C               PRINT 172,(P(I),I=7,12)  HAMF1100
C               PRINT 171
C               PRINT 172,(P(I),I=13,14) HAMF1110
C               ****QUADRUPLE TERM *****
C               DC 402 LL=1,2
C               NL=12+LL          HAMF1120
C               402 A(LL)=F(NL)
C               CALL QUAD(B,A)
C               DC 404 LL=1,2
C               DC 406 LO=1,2          HAMF1130
C               406 A(LO)=0.00
C               A(LL)=1.00
C               CALL QUAD(DA,A)
C               NX=12+LL
C               DC 408 NA=1.36
C               408 CH(NA,NX)=DA(NA)
C               404 CONTINUE
C               $$$$$$ SHFS TERM $$$$$$
C               DC 403 LL=1,6
C               NL=6+LL
C               403 A(LL)=P(NL)
C               CALL SHFS(DA,A)
C               DO 430 LL=1,36
C               430 B(LL)=B(LL)+DA(LL)
C               DO 405 LL=1,6
C               DC 407 LC=1,6
C               407 A(LO)=0.00
C               A(LL)=1.00
C               CALL SHFS(DA,A)
C               DC 409 NA=1.36
C               NX=6+LL

```

IV G LEVEL 21 MAIN DATE = 81171 01/38/83

```

400 OH(NA,NX)=DA(NA)
405 CONTINUE
C          SETTING UP FIELD INDEPENDENT COMPONENTS OF MATRIX ELEMENTS OF H(MATR) AND FIELD INDEPENDENT MATRIX ELEMENTS OF OH(MATR), HA IF1
C          SET-UP THE S-MATRIX
C          TRANSITIONS LOOP STARTS HERE
C          CALCULATE ENERGY DIFFERENCE FROM EXPERIMENTAL FREQUENCY HA IF1
C          CALCULATE COMPONENTS OF FIELD VALUES HA IF1
C
DC 222 LL=1,LW
THETAM=BETA(L)*.0174533
PHIM=ALPHA(L)*.0174533
SINTH=DSIN(THETAM)
COSTH=DCOS(THETAM)
SINPH=DSIN(PHIM)
COSPH=DCOS(PHIM)
X=COSPH*SINTH
Y=SINPH*SINTH
Z=COSTH
PRINT 174, BETA(L),ALPHA(L)
PRINT 175
303 NY=0
DO 322 INDEX=1,11
  IP(HB(L,INDEX),LF,0,0),GC TO 240
  HX=HB(L,INDEX)*X
  HY=HB(L,INDEX)*Y
  HZ=HB(L,INDEX)*Z
  NL=NL+1
C          SETTING UP FIELD DEPENDENT MATRIX ELEMENTS OF H(MATR)
C
C 410 LL=1,6
410 A(LL)=P(LL)
CALL NHAN(A,DA,HX,HY,HZ)
DC 420 LL=1,36
420 P(LL)=DA(LL)+P(LL)
C          SET-UP THE DERIVATIVES OF THE S-MATRIX
DC 412 LL=1,6
DC 414 LCT=1,6
414 A(LCT)=0.00
A(LL)=1.00
CALL NHAN(A,DA,HX,HY,HZ)
DC 415 NH=1,36
415 OH(NH,LL)=DA(NH)
412 CONTINUE
C          CALL CEIGEN DIAGONALIZE COMPLEX MATRIX H(MATR)
C          OBTAIN EIGEN VALUES STORED DIAGONALLY IN H(MATR)
C          OBTAIN EIGENVECTORS STORED IN EVEC(I,E)
C
2500 FORMAT(F(2X,11.6))
NMV=0
CALL CEIGEN (H,EVEC,N,NM)
DC 236 K=1,N
IAREK=(K+1)/2
236 EN(K)=H(IAR)/2.00229
  KW=IP(INDEX)
  NK=JF(INDEX)
  DELTA1=(EN(NK)-EN(K))/HDP(L)
  M=IF(INDEX)
  K=JF(INDEX)
  PRINT 178,I,K,DELTA
C
C          TRANSFORM OH(IAR,I) TO NEW BASIS
C
704 NMV=1
  DC 240 I=1, IMAX
  DC 451 IJ=1, 36
  451 X(IJ)=OH(IJ,I)
  CALL STCH(IJ,DA,EVEC,N,KW,NK)
  DC 460 I=1, 36
  460 OH(IJ,I)=DOP(IJ)
  460 CONTINUE
  XLSF=XLSF+(DELTA1**2)

```

IV G LEVEL 21

MAIN.

DATE = 01171

01/37/59

```

C
C
C           SETTING UP DF(INDEX,I)
C
C   KFW=(K1*KW+K2)/2
C   KW=WK*(WK+1)/2
C   DO 246 I=1,IMAX
C     DE(I)=DHT(KW,I)-DHT(KFW,I)
C
C           .    SETTING UP D1F/DF(I)
C
C   D1F(I)=D1F(I)+(2*DELTA*DE(I))
C 246 CONTINUE
C 243 CONTINUE
C
C           SETTING UP D2F/DP(I)DP(J)
C
C   DO 250 I=1,IMAX
C   DO 250 J=1,IMAX
C   IF (HD(L,INDEX).LE.0.0) GO TO 222
C   IJ=I+(J-1)*IMAX
C   D2E=0.00
C   DO 252 ID=1,N
C     IF (ID.LT.KW) GO TO 256
C     IF (ID.EQ.KW) GO TO 254
C     KID=KW+(ID-ID)/2
C     DHTI=DCCNJG(DHT(KID,I))
C     DHTJ=DHT(KID,J)
C     IT(ID,EC,NK) GO TO 260
C 254 IF (ID.LT.NK) GO TO 258
C     KIDA=NK+(ID-ID)/2
C     DHTIA=DCCNJG(DHT(KIDA,I))
C     DHTJA=DHT(KIDA,J)
C     GC TO 262
C 258 KIDA=ID+(NK*NK-NK)/2
C     DHTI=DHT(KIDA,I)
C     DHTJ=DCCNJG(DHT(KIDA,J))
C     KIDA=ID+(NK*NK-NK)/2
C     DHTIA=DHT(KIDA,I)
C     DHTJA=DCCNJG(DHT(KIDA,J))
C     GO TO 262
C 262 KIDA=ID+(NK*NK-NK)/2
C     DHTIA=DHT(KIDA,I)
C     DHTJA=DCCNJG(DHT(KIDA,J))
C     D2E=D2E+2.00*DHTI*DHTJ/(EN(KW)-EN(ID))
C     GC TO 262
C 264 D2E=D2E+2.00*DHTIA*DHTJA/(EN(NK)-EN(ID))-2.00*DHTI*DHTJ/
C     1 (EN(KW)-EN(ID))
C 265 CONTINUE
C 266 D2F(IJ)=DF(IJ)+(2.00*DE(I)*DE(J))+2.00*DELTA
C 267 CONTINUE
C 222 CONTINUE
NFREE=NL-IMAX
XLSE=XLSE/NFREE
DO 264 I=1,IMAX
  D1F(I)=D1F(I)/NFREE
DO 264 J=1,IMAX
  IJ=I+(J-1)*IMAX
  DCF(IJ)=D2F(IJ)/NF-EF
  D2FINV(IJ)=D2F(IJ)
264 CONTINUE
C
C           CALCULATE AND PRINT PREDICTED DISPLACEMENTS D(I)
PRINT 2000, (D2FINV(IJ),IJ=1,IMAX)
PRINT 2000,(D1F(I),I=1,IMAX)
C
CALL DMINV(D2FINV,JMAX,DET)
2000 FORMAT(2X,14G2.1)
C 266 I=1,IMAX
IJ=I-IMAX
D(I)=0.00
C 266 J=1,IMAX
IJ=IJ+IMAX
D(I)=D(I)-D2FINV(IJ)*D1F(J)
PRINT 180

```

# APPENDIX 5

56

V G LEVEL 31

MAIN

DATE = 81176

22/01/88

```
400  DA(NA,1X)=DA(NA)
405  CONTINUE
```

HAMF1310

```
C C      SETTING UP FIELD INDEPENDENT COMPONENTS OF MATRIX ELEMENTS OF H(IAB) AND FIELD INDEPENDENT MATRIX ELEMENTS OF OH(IAB).HAMF1320
C C      SET-UP THE A-MATRIX
```

HAMF1320

```
C C      TRANSITIONS LOOP STARTS HERE
```

HAMF1340

```
C C      CALCULATE ENERGY DIFFERENCE FROM EXPERIMENTAL FREQUENCY
C C      CALCULATE COMPONENTS OF FIELD VALUES
```

HAMF1730

HAMF1740

HAMF1750

HAMF1760

```
DC 222 L=1,LM
THETAM = PFLA(L) *.0174533
PHIY= ALPHA(L)*.0174533
SINTH=DSIN(THETAM)
COSTH=DCOS(THETAM)
SINPH=DSIN(PHIM)
COSPH=DCOS(PHIM)
Y=COSPH*SINTH
Y=SINPH*SINTH
Z=COSTH
IF (IT,NL,1TM) GC TO 303
PRINT 174, PFLA(L),ALPHA(L)
PRINT 176
```

HAMF1800

HAMF1810

HAMF1820

HAMF1830

HAMF1840

HAMF1850

HAMF1860

```
303  NYE0
DC 222 INDEX=1,11
IF (HBL(L,INDEX).LE.0.) GC TO 248
FY=HBL(L,INDEX)*X
FY=HBL(L,INDEX)*Y
HZ=HBL(L,INDEX)*Z
NL=NL+1
```

HAMF1900

```
C C      SETTING UP FIELD DEPENDENT MATRIX ELEMENTS OF H(IAB)
```

HAMF1930

HAMF1970

HAMF1980

HAMF1990

```
DC 410 LL=1,6
410  A(LL)=P(LL)
CALL HHAM(A,DA,HX,FY,HZ)
DC 410 LL=1,6
411  H(LL)=CA(LL)+C(LL)
C C      SET-UP THE DERIVATIVES OF THE G-MATRIX
DC 412 LL=1,6
DC 414 LCT=1,6
414  A(LL0T)=0.00
A(LL)=1.00
CALLHHAM(A,DA,HX,FY,HZ)
DC 416 NH=1,30
416  F(NH,LL)=DA(NH)
417  CONTINUE
```

HAMF2340

HAMF2350

HAMF2360

HAMF2370

HAMF2380

```
C C      CALL CEIGEN DIAGONALIZE COMPLEX MATRIX H(IAB)
C C      OBTAIN EIGEN VALUES STORED DIAGONALLY IN H(IAB)
C C      OBTAIN EIGENVECTORS STORED IN EVEC(I,E)
```

```
2300 FORMAT(F(2X,112.5))
MV=0
CALL CEIGEN (H,EVEC,N,MV)
DC 235 K=1,N
IAE=K*(K+1)/2
230  EN(K)=F(IAE) /2.00229
K=IE(INDEX)
NK=JE(INDEX)
DELTAF=(EN(NK)-EN(KW))-HCF(L)
ME=IF(INDEX)
KE=JE(INDEX)
IF (IT-NL,1TM) GC TO 304
PRINT 176,M,K,DELTAF
```

HAMF2390

HAMF2400

HAMF2430

HAMF2440

```
C C      TRANSFORM OH(IAB,I) TO NEW BASIS
```

```
234  NMAX=1
        I=1, NMAX
DC 451 J=1, 30
451  DA(I,J)=FH(I,J)
CALL STCM(C,DA,EVEC,N,KW + NK)
DC 452 I=1, 24
452  FH(I,J)=DDO(IF)
```

HAMF2550

HAMF2560

HAMF2570

HAMF2580

V G LEVEL 21

MAIN

DATE = 81176

22/01/88

240 CONTINUE

XLSEF=XLSEF+(DELTAX\*\*2) ----- HAMF2750

C

C

C

C

SETTING UP DE(INDEX,I)

HAMF2760

HAMF2770

HAMF2780

HAMF2790

HAMF2800

HAMF2805

HAMF2810

HAMF2820

HAMF2830

HAMF2840

HAMF2950

HAMF2960

HAMF2970

HAMF2980

HAMF2990

HAMF3000

HAMF3010

HAMF3020

HAMF3030

HAMF3040

HAMF3050

HAMF3060

HAMF3070

HAMF3080

HAMF3090

HAMF3100

HAMF3110

HAMF3120

HAMF3130

HAMF3140

HAMF3150

HAMF3160

HAMF3170

HAMF3180

HAMF3190

HAMF3200

HAMF3210

HAMF3220

HAMF3230

HAMF3240

HAMF3250

HAMF3270

HAMF3280

HAMF3290

HAMF3300

HAMF3310

HAMF3320

HAMF3330

HAMF3340

HAMF3350

HAMF3360

HAMF3370

HAMF3380

HAMF3390

240 CONTINUE

XLSEF=XLSEF+(DELTAX\*\*2) ----- HAMF2750

C

C

C

C

SETTING UP C1F/CP(I)

241 C1F(I)=C1F(I)+(2\*DELTAX\*DE(I))  
242 CONTINUE  
243 CONTINUE

SETTING UP D2F/CF(I)DP(J)

244 250 I=1,IMAX  
250 J=1,IMAX  
IF (I>L,INDEX).LE.0.01 GO TO 222

IJK=I+(J-1)\*IMAX

DE=0.00

252 IJK=1,N

IF (ID.LT.KW) GO TC 256

IF (ID.EC.KW) GO TC 254

K1D=KW+(ID-ID-IC)/2

CHTI=DCCONJG(DHT(K1C,I))

CHTJA=DHT(K1J,J)

IF (IJ.LT.NK) GO TC 260

IF (I.J.LT.NK) GO TC 258

K1CA=NKA+(ID-ID-IC)/2

CHTIA=DCCONJG(DHT(K1A,I))

CHTJA=DHT(K1A,J)

GO TC 262

254 K1D=ID+(NK-NK-NK)/2

CHTIA=DHT(K1D,I)

CHTJA=DCCONJG(DHT(K1D,J))

K1CA=I,(NKA-NK-NK)/2

CHTIA=DHT(K1A,I)

CHTJA=DCCONJG(DHT(K1A,J))

GO TU 262

258 K1CA=ID+(NK-NK-NK)/2

CHTIA=DHT(K1A,I)

CHTJA=DCCONJG(DHT(K1A,J))

DE=0.25\*(DHTIA\*DHTJA/(EN(NK)-EN(ID))-2.00\*DHTIA\*DHTJA/(EN(KW)-EN(ID)))

GO TU 262

262 DE=0.25\*(DHTIA\*DHTJA/(EN(NK)-EN(ID))-2.00\*DHTIA\*DHTJA/(EN(KW)-EN(ID)))

1 (EN(KA)-EN(ID))

263 CONTINUE

DE(IJ)=DE(IJ)+(2.00\*DE(I)\*DE(J))+DE\*DELTAX

265 CONTINUE

222 CONTINUE

NFRCE=NL-IMAX

XLSEF=XLSEF/NFRCE

264 I=1,IMAX

IJ=I+(J-1)\*IMAX

DE(IJ)=DE(IJ)/NFRCE

DEINV(IJ)=DE(IJ)

264 CONTINUE

C

C

C

C

C

C

C

C

C

C

C

C

C

C

C

C

C

C

C

C

C

C

C

C

C

C

C

C

C

C

C

C

C

C

C

C

C

C

C

C

C

C

C

C

C

C

C

C

C

C

C

C

C

C

C

C

C

C

C

C

C

C

C

C

C

C

C

C

C

C

C

C

C

C

C

C

C

C

C

C

C

C

C

C

C

C

C

C

C

C

C

C

C

C

C

C

C

C

C

C

C

C

C

C

C

C

C

C

C

C

C

C

C

C

C

C

C

C

C

C

C

C

C

C

C

C

C

C

C

C

C

C

C

C

C

C

C

C

C

C

C

C

C

C

C

C

C

C

C

C

C

C

C

C

C

C

C

C

C

C

C

C

C

C

C

C

C

C

C

C

C

C

C

C

C

C

C

C

C

C

C

C

C

C

C

C

C

C

C

C

C

C

C

C

C

C

C

C

C

C

C

C

C

C

C

C

C

C

C

C

C

C

C

C

C

C

C

C

C

C

C

V G LEVEL 21 MAIN DATE = 81176 22/01/83

```

260 C(I)=D(I)-D2FINV(IJ)*C1F(J) HAMF3470
PRINT 160 HAMF3480
PRINT 161,(D(I),I=1,12) HAMF3490
PRINT 162
PRINT 163,(C(I),I=12,IMAX)

      CALCULATE AND PRINT NEW VALUES FOR PARAMETERS P(I) HAMF3500
      HAMF3510
      HAMF3520
      HAMF3530
      HAMF3540
      HAMF3550

260 D( I )=P( I )+C( I )
PRINT 164
PRINT 165
PRINT 166,(P( I ),I=1,6)
PRINT 167
PRINT 168,(P( I ),I=7,12)
PRINT 169
PRINT 170,(P( I ),I=13,14)
XLSNF=XLSP
II=IMAX
DO 270 I=1,IMAX
II=II+1MAX+1
XLSNEW=XLSP+D1F(I)*D(I)+(D2F(II)*C(I)*D(I))/2.00
JN=I+1
IF(I.GE.1MAX) GO TO 270
DO 272 J=J**IN,IMAX
IJ=II-I+J
XLSNEW=XLSNEW+D2F(IJ)*C(I)*D(J)
272 CONTINUE
270 CONTINUE

      CHECK FOR CONVERGENCE OF P(I) HAMF3560
      HAMF3590
      HAMF3600
      HAMF3610
      HAMF3620
      HA 1F3630
      HAMF3640
      HAMF3650
      HAMF3660
      HAMF3670
      HAMF3680
      HAMF3690
      HAMF3700
      HA 1F3710
      HAMF3720
      HAMF3730
      HAMF3740
      HAMF3750
      HAMF3760
      HAMF3770
      HAMF3780
      HAMF3790
      HAMF3800
      HA 1F3810
      HAMF3820
      HAMF3830

      CALCULATE SIGMA(I) HAMF3840
      HAMF3850
      HAMF3860
      HAMF3870
      HAMF3880
      HAMF3890
      HAMF3900
      HAMF3910
      HAMF3920
      HAMF3930

274 SIGMA(I)=DSQRT(DABS(D2FINV(II)*XLSNEW*2.00/NFREE))
CNG=DSQRT(XLSP)
RMSNEW=DSQRT(XLSNEW)
PRINT 186
PRINT 169
PRINT 172,(SIGMA(I),I=1,6)
PRINT 173
PRINT 174,(SIGMA(I),I=7,12)
PRINT 175
PRINT 176,(SIGMA(I),I=13,14)
PRINT 180,2NS,RMSNEW,NL
274 CONTINUE
IF (INCNE) 1000,1001,1000 HAMF3850
1001 CONTINUE
STOP HAMF3860
END HAMF3870

```

Subroutine: CEIGEN

Purpose: Compute eigenvalues and eigenvectors of a Hermitean matrix (double precision complex).

Usage: CALL CEIGEN (A,R,N,MV).

Description of parameters:

A - (COMPLEX \* 16) original Hermitean matrix, destroyed during computation. Upon return, A is the diagonalized matrix with storage in use; the upper right side of the matrix actually stores: the (I,J) element is the  $I + (J * J - J)/2$  element of A for  $I < J$ . For  $I > J$  the (I,J) element is the complex conjugate of the (J,I) element, i.e. of the  $J + (I * I - I)/2$  member of A.

R - (COMPLEX \* 16) the unitary transformation which diagonalizes A. The columns of R are eigenvectors of A ordered as are the eigenvalues.

N - the order (dimension) of A and R

MV - input code:

O compute eigenvalues and eigenvectors  
I compute eigenvalues only. (R need not  
be dimensioned but must still appear in  
calling sequence.)

Method: an extension of the Jacobi method to Hermitean matrices as given, for example in C.-E Froberg, 'Introduction to Numerical Analysis' (Addison-Wesley, 1965) p. 111. The coding parallels that for EIGEN (see publication 360ACM, p. 165).

Programmed by: Wm. E. Bavlis,  
Physics Department,  
University of Windsor.

Execution time: 0.5 sec CPU on the IBM 360 Model 50 of University of Windsor for  $N = 4$ . The time will vary roughly as  $N^4$  but will be less if some off-diagonal elements of A are initially = 0.

Page 59  
MISSING

## APPENDIX 6

61

\$JOB LIST XXXXXXXXX UNWIN

COMPUTES DOUBLE PRECISION EIGENVALUES AND, UNLESS MV=1, ALSO COMPLEX EIGENVECTORS OF THE HERMITEAN MATRIX CA OF DIMENSION N. THE JACOBI METHOD IS USED.

THE CALLING PARAMETERS ARE:

- CA - THE HERMITEAN MATRIX TO BE DIAGONALIZED. COMPACT STORAGE IS USED. NAMELY THE (I,J)TH ELEMENT OF THE UPPER RIGHT HALF OF THE HERMITEAN MATRIX IS ELEMENT I+(J\*J-J)/2 OF CA.
- CR - THE INPUT VALUES OF THIS MATRIX ARE NOT USED. UPON RETURN, IF MV .NE. 1, CR CONTAINS THE COMPLEX EIGENVECTORS OF THE INPUT CA MATRIX. THE EIGENVECTORS ARE STORED COLUMNWISE IN THE SAME SEQUENCE AS THE EIGENVALUES.
- N - THE DIMENSION OF THE MATRIX TO BE DIAGONALIZED.
- MV - IF EQUAL TO 1, ONLY EIGENVALUES AND NOT EIGENVECTORS ARE COMPUTED.

W. E. BAYLIS, PHYSICS, U. WINDSOR, WINDSOR, ONTARIO. FEB. 1972

```

IMPLICIT REAL*8 (A,D,G,O-Z), COMPLEX*16(C)
COMPLEX*16 ONE/(1.000,0.000)/,ZERO/(0.000,0.000)/
COMPLEX*16 DCCNJC
REAL*8 CDABS
REAL*8 COSP,COSP2
DIMENSION CA(1),CR(1),CSINP(2)

C CHECK DIMENSION
IF(N-1).LT.5
1 PRINT 200,N
200 FORMAT(' ERROR. ATTEMPT TO DIMENSION CEIGEN BY N>.'I6.'.'//'
          ' EXECUTION.')
      STOP
2 IF(MV .EQ. 1) GO TO 4.
CR(1) = ONE
4 RETURN

C GENERATE IDENTITY MATRIX
5 RANGE = 1.0D-12
IF(MV .EQ. 1) GO TO 25
IQ = -1
DO 20 J=1,N
IQ = IC + N
DO 20 I=1,N
IJ = IC + I
CR(IJ) = ZERO
IF(I .EQ. J) CR(IJ) = ONE
20 CONTINUE

C COMPUTE INITIAL AND FINAL NORMS
25 ANORM = 0.0D0
Y = 0.0D0
IJ = 0
DO 35 J=1,N
DO 35 I=1,J
IJ = IJ + 1
X = CA(IJ)*DCCNJC(CA(IJ))
ANORM = ANORM + X
IF(I .EQ. J) GO TO 35
Y = Y + X
35 CONTINUE
ANORM = 1.414D0*DSQRT(ANORM)
ANRMX = ANORM*RANGE/DFLOAT(N)
IF(Y .LE. ANRMX) GO TO 165

C INITIALIZE INDICATORS AND COMPUTE THRESHOLD: :THR:
IND = 0
THR = ANORM
45 THR = THR/DFLOAT(N)
50 L=1
55 M=L+1
LO = (L*L-L)/2
LL = LC + L

```

```

ILO = N*(L-1)          00012000
60 MJ = (N*M-M)/2      00012100
LM = L + MJ            00012200
C COMPUTE ELEMENTS OF 2X2 ROTATION MATRIX IF OFF-DIAGONAL ELEMENT IS 00012300
C LARGER THAN THR        00012400
C
GAM = CDABS(CA(LM))    00012500
IF(GAM .LT. THR) GO TO 130 00012600
MM = MJ + M            00012700
IMQ = N*(M-1)           00012800
IND = 1                 00012900
X = CA(LM)              00013000
IF(X .LT. 0.0D0) GAM = -GAM 00013100
X = (CA(LL) - CA(MM))/2.0D0 00013200
Y = GAM/DSQRT(X*X+GAM*GAM) 00013300
IF(X .LT. 0.0D0) Y = -Y 00013400
SINP = X/DSQRT(2.0D0*41.0D0 + CSQRT(1.0D0 - Y*Y))) 00013500
SINP2 = SINP*SINP        00013600
COSP2 = 1.0D0 - SINP2     00013700
COSP = DSQRT(COSP2)      00013800
CSINP(1) = GAM*SINP/CA(LM) 00013900
CSINP(2) = DCLNJG(CSINP(1)) 00014000
GSIN2P = 2.0D0*GAM*SINP*COSP 00014100
C
ROTATE COLUMNS AND ROWS L AND M 00014200
C
IQ = 0                 00014300
DO 125 I=1,N           00014400
IQ = IC + I - 1         00014500
IF(I-M) 85.115.90       00014600
85 IM = I + MO          00014700
MCONJ = 1               00014800
IF(I-L) 100.115.105     00014900
100 IL = I + IQ          00015000
LCCNJ = 1               00015100
GO TO 110               00015200
90 IM = M + IQ          00015300
MCCNJ = 2               00015400
105 IL = L + IQ          00015500
LCCNJ = 2               00015600
GO TO 110               00015700
90 IM = M + IQ          00015800
MCCNJ = 2               00015900
105 IL = L + IQ          00016000
LCCNJ = 2               00016100
110 CX = CA(IM)*CSINP(MCONJ) 00016200
CY = CA(IL)*CSINP(3-LCCNJ) 00016300
IF(MCONJ .EQ. LCCNJ) GO TO 112 00016400
CA(IL) = CA(IL)*CCSP + LCCNJG(CX) 00016500
CA(IM) = CA(IM)*CCSP - LCCNJG(CY) 00016600
GO TC 115               00016700
112 CA(IL) = CA(IL)*CCSP + CX 00016800
CA(IM) = CA(IM)*CCSP - CY 00016900
115 IF(MV .EQ. 1) GO TO 125 00017000
ILR = ILQ + I            00017100
IMR = IMQ + I            00017200
CX = CR(ILR)*CCSP + CR(1MR)*CSINP(1) 00017300
CR(IMR) = CR(IMR)*COSP - CR(ILR)*CSINP(2) 00017400
CR(ILR) = CX             00017500
125 CCNTINUE
X = CA(LL)*SINP2 + CA(MM)*COSP2 - GSIN2P 00017600
CA(LL) = CA(MM)*SINP2 + CA(LL)*COSP2 + GSIN2P 00017700
CA(MM) = X               00017800
CA(LM) = ZERO             00017900
130 IF(M .EQ. N) GO TC 140 00018000
M = M+1                  00018100
GO TO 60                 00018200
140 IF(L .EQ. N-1) GO TO 150 00018300
L = L+1                  00018400
GO TO 55                 00018500
150 IF(IND .EQ. 0) GO TO 150 00018600
IND = 0                  00018700
GO TO 50                 00018800
160 IF(THR .GT. ANPMX) GO TO 45 00018900
C
C SORT EIGENVALUES AND EIGENVECTORS 00019000
C
165 IQ = -K              00019100
LL=0                      00019200
JC 185      I = 1,N      00019300
IQ = IC + N              00019400
LL = LL + I              00019500
JO = N*(I-2)              00019600
X = CA(LL)                00019700
JO = N*(I-2)              00019800
X = CA(LL)                00019900

```

```
DO 185 J=I,N          00020000
  JQ = JQ + N          00020100
  MM = (J*J+J)/2      00020200
  Y= CA(MM)           00020300
  IF(X .LE. Y) GO TO 185 00020400
  CA(LL) = Y          00020500
  CA(MM) = X          00020600
  X = Y               00020700
  IF(MV .EQ. 1) GO TO 185 00020800
  DO 180 K=1,N          00020900
    ILR = IQ + K        00021000
    IMR = JQ + K        00021100
    CX = CR(ILR)       00021200
    CR(ILR) = CR(IMR)  00021300
  180 CR(IMR) = CX      00021400
  185 CONTINUE          00021500
  RETURN               00021600
END                  00021700
```

# APPENDIX 7

64

```
1 SJOB LIST XXXXXXXXXX UNW IN
2 SUBROUTINE DGMPRE(A,B,R,N,M,L)
3 IMPLICIT REAL(A-H,O-Z)
4 DIMENSION A(144),E(144),R(144)
5 IR=0.DC
6 IK=-N
7 DO 10 K=1,L
8 IK=IK+N
9 DO 10 J=1,N
10 IR=IR+1
11 JI=J-N
12 IB=IK
13 R(IR)=0.D0
14 DO 10 I=1,M
15 JI=JI+N
16 IB=IB+1
17 10 R(IR)=R(IR)+A(JI)*B(IB)
18 RETURN
19 END
//
```

//W JOB (U10200S538),CLASS=W  
//W JCB (U10200S538),CLASS=W

JOB 787  
JOB 787

## APPENDIX 8

## DIAGONALIZATION OF g AND A TENSORS

The computer program used to evaluate the principal axes and values of the g and A tensors is shown overleaf. The program forms a traceless tensor and then employs three rotations to diagonalize this tensor.

## APPENDIX 8

```

1 JOB      WATFIV'>>>>xxx, KP=26 F HELLO
2 DIMENSION G(3),D(3),C(3,3),U(3,3),VV(3)
3 READ 3,XX,YY,ZZ,X,Y,Z,X,Y,Z
4 FORMAT (EF10.5)
5 XZ=ZX
6 YX=XY
7 ZY=YZ
8 PI=PI./E7.296
9 P=-((XX+YY+ZZ))
10 U=(XX*YY+XX*ZZ+YY*ZZ-YZ**2-XY**2-XZ**2)
11 R=-(XX*ZZ*YY+2.*XY*YZ*ZX-YZ**2*XX-XY**2*ZZ-ZX**2*YY)
12 A=(3.*P-P**2)/3.
13 A=-A
14 R=(2.*A+3.-S.*P*Q+27.*Q)/27.
15 D=-S
16 M=AES (P)
17 CC=(PP/2.)*{SORT((3./A)**3)}
18 SI=SORT (1.-CC**2)
19 CS=AES (C)
20 PHI=ATAN (SI/CS)
21 IF(CC) 50,51,51
22 50 PHI=PI-PHI
23 51 ALPHA=PHI/3.
24 AA=2.*SORT (A/3.)
25 G(1)=AA*COS (ALPHA-2.*PI*1./3.)
26 G(2)=AA*COS (ALPHA-2.*PI*2./3.)
27 G(3)=AA*COS (ALPHA-2.*PI*3./3.)
28 PHI=PHI+E7.296
29 ALPHA=ALPHA+E7.296
30 AS=-P/S.
31 PRINT 1,(G(1),G(2),G(3),AS
32 G(1)=(G(1)-P/3.)
33 G(2)=(G(2)-P/3.)
34 G(3)=(G(3)-P/3.)
35 DO 10 L=1,3
36 D(1)=XY*YZ-ZX*(YY-G(L))
37 D(2)=ZX*YY-YZ*(XX-G(L))
38 D(3)=(XX-G(L))**2+(YY-G(L))**2+D(3)**2
39 DD=SORT (D(1)**2+D(2)**2+D(3)**2)
40 U(1,L)=D(1)/DD
41 U(2,L)=D(2)/DD
42 10 U(3,L)=D(3)/DD
43 PI=INT 1,(G(1),G(2),G(3),PHI,ALPHA
44 DO 11 N=1,3
45 11 PRINT 1,U(1,N),U(2,N),U(3,N)
46 DO 12 L=1,3
47 12 DO 13 N=1,2
48 13 SI=SORT (1.-U(N,L)**2)
49 C(N,L)=ATAN (SI/U(N,L))
50 C(N,L)=C(N,L)+E7.296
51 13 CONTINUE
52 VV(1)=U(1,L)
53 VV(2)=U(2,L)
54 VV(3)=U(3,L)
55 TANA=AES (VV(2)/VV(1))
56 ALPHA=ATAN (TANA)
57 IF(VV(1))101,103,105
58 100 IF(VV(2))104,106,107
59 104 ALPHA=-ALPHA
60 105 GO TO 107
61 101 IF(VV(1))102,103,103
62 102 ALPHA=-1+E0./E7.296+ALPHA
63 GO TO 107
64 103 ALPHA=1+E0./E7.296-ALPHA
65 107 WM=AES (VV(3))
66 TANB=SORT (1.-VV(3)**2)/WM
67 BETHA=ATAN (TANB)
68 IF(VV(3)) 108,109,109
69 108 BETHA=100./E7.296-BETHA
70 109 BETHA=BETHA+E7.296
71 ALPHA=ALPHA+E7.296
72 PI=INT 1,(G(1,N),N=1,3),ALPHA,BETHA
73 12 CONTINUE
74 1 FORMAT(2FX,2F10.5)
75 STOP
76 END

```

SENTRY

2.70369 2.0121" 2.04221 0.00811 0.00755 0.01354

## VITA AUCTORIS

I was born in Loughborough, Leicestershire, in 1959.  
I completed my secondary education at Hind Leys College Shepsled  
and Burleigh Community College Loughborough. I graduated from  
Queens' College in the University of Cambridge in 1980 with a  
B.A. in Physics. At present I am completing requirements  
towards my MSc at the University of Windsor, Ontario.

PAGE 67 MISSING